Neurobiology of Disease

14-3-3 Proteins Reduce Cell-to-Cell Transfer and Propagation of Pathogenic α-Synuclein

Bing Wang,[1] **Rachel Underwood,**[1] **Anjali Kamath,**[1] **Colleen Britain,**[1] **Michael B. McFerrin,**[1] ⬤**Pamela J. McLean,**[3]
Laura A. Volpicelli-Daley,[1] **Robert H. Whitaker,**[2] ⬤**William J. Placzek,**[2] **Katelyn Becker,**[4] **Jiyan Ma,**[4] and
Talene A. Yacoubian[1]

[1]Center for Neurodegeneration and Experimental Therapeutics, Department of Neurology, [2]Department of Biochemistry and Molecular Genetics, University of Alabama at Birmingham, Birmingham, Alabama 35294, [3]Department of Neuroscience, Mayo Clinic, Jacksonville, Florida 32224, and [4]Center for Neurodegenerative Science, Van Andel Research Institute, Grand Rapids, Michigan 49503

α-Synuclein (αsyn) is the key protein that forms neuronal aggregates in the neurodegenerative disorders Parkinson's disease (PD) and dementia with Lewy bodies. Recent evidence points to the prion-like spread of αsyn from one brain region to another. Propagation of αsyn is likely dependent on release, uptake, and misfolding. Under normal circumstances, this highly expressed brain protein functions normally without promoting pathology, yet the underlying endogenous mechanisms that prevent αsyn spread are not understood. 14-3-3 proteins are highly expressed brain proteins that have chaperone function and regulate protein trafficking. In this study, we investigated the potential role of the 14-3-3 proteins in the regulation of αsyn spread using two models of αsyn spread. In a paracrine αsyn model, 14-3-3θ promoted release of αsyn complexed with 14-3-3θ. Despite higher amounts of released αsyn, extracellular αsyn showed reduced oligomerization and seeding capability, reduced internalization, and reduced toxicity in primary mixed-gender mouse neurons. 14-3-3 inhibition reduced the amount of αsyn released, yet released αsyn was more toxic and demonstrated increased oligomerization, seeding capability, and internalization. In the preformed fibril model, 14-3-3 θ reduced αsyn aggregation and neuronal death, whereas 14-3-3 inhibition enhanced αsyn aggregation and neuronal death in primary mouse neurons. 14-3-3s blocked αsyn spread to distal chamber neurons not exposed directly to fibrils in multichamber, microfluidic devices. These findings point to 14-3-3s as a direct regulator of αsyn propagation, and suggest that dysfunction of 14-3-3 function may promote αsyn pathology in PD and related synucleinopathies.

Key words: 14-3-3 proteins; aggregation; α-synuclein; dementia with Lewy bodies; exosome; Parkinson's disease

---

Significance Statement

Transfer of misfolded aggregates of α-synuclein from one brain region to another is implicated in the pathogenesis of Parkinson's disease and other synucleinopathies. This process is dependent on active release, internalization, and misfolding of α-synuclein. 14-3-3 proteins are highly expressed chaperone proteins that interact with α-synuclein and regulate protein trafficking. We used two different models in which toxicity is associated with cell-to-cell transfer of α-synuclein to test whether 14-3-3s impact α-synuclein toxicity. We demonstrate that 14-3-3θ reduces α-synuclein transfer and toxicity by inhibiting oligomerization, seeding capability, and internalization of α-synuclein, whereas 14-3-3 inhibition accelerates the transfer and toxicity of α-synuclein in these models. Dysfunction of 14-3-3 function may be a critical mechanism by which α-synuclein propagation occurs in disease.

Introduction

α-Synuclein (αsyn) is the key protein implicated in the pathogenesis of Parkinson's disease (PD) and dementia with Lewy bodies

(DLB). Recent evidence points to the possibility that αsyn has prion-like properties. Fetal grafts transplanted into PD patients

develop αsyn aggregates, suggesting cell-to-cell transmission of the disease process, and stem cells transplanted into mice overexpressing αsyn show similar effects (Kordower et al., 2008; Desplats et al., 2009; Hansen et al., 2011). αSyn protofibrils cause aggregation of endogenous αsyn and neuronal death in primary neuronal culture (Volpicelli-Daley et al., 2011), and fibrils injected into rodent striatum leads to αsyn aggregation in the substantia nigra (SN) with subsequent dopaminergic loss and aggregation in other brain regions including the amygdala and frontal cortex (Luk et al., 2012; Masuda-Suzukake et al., 2014; Paumier et al., 2015; Abdelmotilib et al., 2017). Transmission of pathologic αsyn likely depends on misfolding, release, and uptake of αsyn. Potential cellular mechanisms implicated in αsyn release include exosomal and non-exosomal secretion pathways and transfer through tunneling nanotubes, among other possible mechanisms (Lee et al., 2005; Liu et al., 2009; Emmanouilidou et al., 2010; Hasegawa et al., 2011; Danzer et al., 2012; Abounit et al., 2016). The endogenous mechanisms that normally prevent the spread of the highly abundant αsyn are not well elucidated.

14-3-3 proteins comprise a family of seven conserved proteins that are highly expressed in the brain. These proteins are critical to neuronal function through their roles affecting protein folding, protein trafficking, and neurite growth among other functions (Vincenz and Dixit, 1996; Mrowiec and Schwappach, 2006; Yano et al., 2006; Kajiwara et al., 2009; Ramser et al., 2010; Shandala et al., 2011; Winter et al., 2012; Yoon et al., 2012; Marzinke et al., 2013; Foote et al., 2015; Lavalley et al., 2016; Kaplan et al., 2017; Sluchanko and Gusev, 2017). 14-3-3s interact with key proteins implicated in PD, including αsyn, parkin, and LRRK2 (Ostrerova et al., 1999; Xu et al., 2002; Sato et al., 2006; Dzamko et al., 2010; Nichols et al., 2010; Li et al., 2011). 14-3-3s colocalize with αsyn in Lewy Bodies in both PD and DLB (Kawamoto et al., 2002; Berg et al., 2003). Our work reveals a reduction of 14-3-3 levels in cellular and mouse αsyn models and in the temporal cortices of patients with DLB (Yacoubian et al., 2008, 2010; Ding et al., 2013; McFerrin et al., 2017). Transcriptional analysis of PD patients points to 14-3-3s as a critical hub of dysregulated proteins in PD (Ulitsky et al., 2010). 14-3-3 overexpression is protective in neurotoxin and LRRK2 models, whereas 14-3-3 inhibition with the pan 14-3-3 inhibitor promotes toxicity (Yacoubian et al., 2010; Slone et al., 2011, 2015; Ding et al., 2015; Lavalley et al., 2016).

Because of their functions in protein folding and protein trafficking, we hypothesized that 14-3-3s regulate αsyn transmission. Certain 14-3-3 isoforms, particularly 14-3-3θ, reduce fibrillization of recombinant αsyn in vitro (Plotegher et al., 2014). 14-3-3s regulate non-classical protein secretion in association with the GTPase Rab11 (Shandala et al., 2011), a Rab protein previously shown to promote αsyn secretion (Liu et al., 2009; Chutna et al., 2014; Goncalves et al., 2016). 14-3-3s also mediate exosomal release of LRRK2 (Fraser et al., 2013). We propose that 14-3-3s serve as part of an endogenous system that normally prevents αsyn transmission, yet under disease condition, lower levels of 14-3-3s are unable to handle excess αsyn. Here we examine the effect of 14-3-3 proteins, with an emphasis on 14-3-3θ, on αsyn toxicity in two separate αsyn models, and evaluate 14-3-3s' impact on αsyn release, oligomerization, seeding, and internalization. We found that 14-3-3θ prevents αsyn transmission and

neuron death by reducing αsyn oligomerization, seeding, and internalization despite increasing total αsyn release.

Materials and Methods

Mice. Mice were used in accordance with the guidelines of the National Institute of Health (NIH) and University of Alabama at Birmingham (UAB) Institutional Animal Care and Use Committee (IACUC). Animal work performed in this study was approved by UAB's IACUC. Transgenic mice expressing human 14-3-3θ tagged with a hemagglutinin (HA) epitope tag at the C-terminal end under the neuronal promoter Thy1.2 were previously developed in our laboratory (Lavalley et al., 2016). Transgenic mice expressing difopein-enhanced yellow fluorescent protein (eYFP) under the neuronal promoter Thy1.2 were obtained from Dr. Yi Zhou at Florida State University (Qiao et al., 2014). 14-3-3θ hemizygous mice and difopein hemizygous mice were bred with C57BL/6J mice from The Jackson Laboratory (catalog #000664; RRID:IMSR_JAX:000664).

Cell lines. Isyn cells were previously created by infecting SK-N-BE(2)-M17 (M17) male neuroblastoma cells (obtained and authenticated by ATCC; catalog #CRL-2267; RRID:CVCL_0167) with the doxycycline-inducible αsyn pSLIK lentivirus in the presence of 6 μg/ml polybrene followed by selection for stable transfection with G418 (Slone et al., 2015). Isyn cells were maintained in 1:1 Eagle's MEM/F12K containing 10% fetal bovine serum (FBS), 1% penicillin/streptomycin, and G418 (500 μg/ml) at 37°C. To induce αsyn expression, cells were treated with doxycycline (doxy) at 10 μg/ml.

To create isyn/14-3-3θ, isyn/14-3-3ζ, isyn/difopein-eYFP, or isyn/mutant difopein-eYFP lines, isyn cells were transduced with the doxy-inducible 14-3-3θ, 14-3-3ζ, difopein-eYFP, or mutant difopein-eYFP pSLIK-hygro lentiviruses, followed by selection for stable transfection with hygromycin (100 μg/ml) in addition to G418. The difopein-eYFP and mutant difopein-eYFP pSLIK constructs were created by the UAB Neuroscience Core Center by first cloning difopein-eYFP or mutant difopein-eYFP into the pEN_TTmcs vector, followed by recombination with the hygromycin-selectable pSLIK lentiviral construct (Shin et al., 2006). The 14-3-3θ and 14-3-3ζ pSLIK constructs were similarly constructed. Lines were maintained in 1:1 Eagle's MEM/F12K containing 10% FBS, 1% penicillin/streptomycin, G418 (500 μg/ml), and hygromycin (100 μg/ml) at 37°C. To induce expression, cells were treated with doxy at 10 μg/ml.

SH-SY5Y cells were obtained and authenticated by ATCC (Cat #CRL-2266 RRID:CVCL_0019). SH-SY5Y cells were maintained in 1:1 Eagle's MEM/F12K containing 10% FBS, and 1% penicillin/streptomycin. For differentiation, SH-SY5Y cells were treated with retinoic acid (10 μM) for 5–7 d.

H4 neuroglioma cells were obtained and authenticated by ATCC (catalog #HTB-148; RRID:CVCL_1239). H4 cells were maintained in OptiMEM media with 10% FBS.

Primary neuronal culture preparation. Hippocampi or cortices were dissected from male and female postnatal day (P)0 mice and incubated in papain for 25 min at 37°C. Cells were thoroughly washed using neurobasal-A media containing B-27 supplement and 5% FBS before tituration using fire polished glass pipettes. After centrifugation at 1500 rpm for 5 min, the cell pellet was layered on 4% BSA in HBSS and centrifuged at 700 rpm for 5 min. Resuspended cells were plated on 18 mm glass coverslips coated with poly-D-lysine. After 12–16 h, media was replaced by neurobasal-A media containing B-27 supplement and Arabinose C at 6 μM. Fifty percent media changes were made every 7 d.

For preformed fibril (PFF) experiments, neurons underwent a complete media change and were treated with PBS, monomeric human αsyn, or human αsyn PFFs in neurobasal-A media with B-27 supplement at 5 d in vitro (DIV).

Preparation of conditioned media. For preparation of conditioned media (CM), isyn cells were switched to serum-free Eagle's MEM/F12K. At time of collection, CM was removed from cells and then underwent serial centrifugations at 800 g for 5 min, then at 2000 × g for 10 min, and then at 10,000 × g for 30 min at 4°C to remove cellular debris. For Western blot analyses, CM was then concentrated using a 3 kDa Amicon Ultra-4 centrifugal filter at 4000 × g for 2 h and then dialyzed. Protein concentrations of CM samples were assessed by BCA assay (ThermoFisher Sci-

Correspondence should be addressed to Dr. Talene A. Yacoubian, Civitan International Research Center 560D, 1719 6th Avenue South, Birmingham, AL 35294. E-mail: tyacoubian@uabmc.edu.

entific), and equal protein amounts were loaded for each CM sample for Western blot analysis.

For toxicity experiments, isyn cells were induced with doxycycline in Eagle's MEM/F12K with 10% FBS for 1 week and then switched to serum-free Eagle's MEM/F12K for 48 h. Collected CM underwent centrifugation at $800 \times g$ for 5 min, then at $2000 \times g$ for 10 min, and then at $10,000 \times g$ for 30 min before transfer to primary neuronal cultures or differentiated SH-SY5Y cells.

14-3-3θ knockdown. The pLKO.1–14-3-3θ shRNA lentiviral vectors were originally purchased from Open Biosystems and previously tested for efficacy in reducing 14-3-3θ protein expression (Yacoubian et al., 2010). Isyn cells were transduced with the empty vector pLKO.1 virus or 14-3-3θ shRNA virus previously shown to have high efficacy in 14-3-3θ protein knockdown in the presence of 6 μg/ml polybrene. Transduced cells were selected with 2 μg/ml puromycin 72 h later.

Ethidium D cell death assay. Cells were rinsed in PBS and then incubated in 1 μM ethidium D and 2 μg/ml Hoechst 33342 in culture media for 30 min at 37°C. Ten high-power (20×) fields per well were randomly selected for quantification, and the number of ethidium D-positive cells and the total number of cells stained by Hoechst 33342 were counted per high-power field with the rater blind to experimental conditions.

Western blot. Cell pellets were sonicated in lysis buffer (150 mM NaCl, 10 mM Tris-HCl, pH 7.4, 1 mM EGTA, 1 mM EDTA, 0.5% NP-40, protease inhibitor cocktail; ThermoFisher Scientific) and then underwent centrifugation at $16,000 \times g$ for 10 min. Protein concentrations were assessed by BCA assay (ThermoFisher Scientific). Cell lysate and CM samples were boiled in 4× DTT sample loading buffer (0.25 M Tris-HCl, pH 6.8, 8% SDS, 200 mM DTT, 30% glycerol, Bromophenol Blue). Equal protein amounts were loaded per well for the CM samples and for cell lysate samples, resolved on 12% SDS-polyacrylamide gels, and transferred to nitrocellulose membranes. After blocking in 5% nonfat dry milk in TBST (25 mM Tris-HCl, pH 7.6, 137 mM NaCl, 0.1% Tween 20), membranes were incubated overnight in primary antibody at 4°C and then in HRP-conjugated goat anti-mouse or anti-rabbit secondary antibodies (1:2000; Jackson ImmunoResearch) for 2 h. Primary antibodies used are listed in Table 1. After washing in TBST six times, blots were developed with enhanced chemiluminescence method (GE Healthcare). Images were scanned and analyzed using Un-ScanIT software for densitometric analysis of bands.

Immunoprecipitation. Ten microliters of protein G-conjugated Dynabeads (ThermoFisher Scientific) were incubated overnight with mouse IgG, mouse monoclonal antibody against αsyn (final concentration 0.5 or 1 μg/ml; BD Biosciences, 610787), or mouse monoclonal against V5 (final concentration 10 μg/ml; ThermoFisher Scientific, R960-25) before adding to CM. Antibody-coupled Dynabeads was incubated with 3 ml CM overnight. CM after immunodepletion was then used for toxicity assays.

ELISA. αSyn levels in CM were measured using an ELISA for αsyn (ThermoFisher Scientific), according to the manufacturer's instructions.

Exosome fractionation. For exosome preparation, we followed the protocol described in (Thery et al., 2006). Briefly, cells were incubated to serum-free Eagle's MEM/F12K for 96 h. CM underwent serial centrifugations at $800 \times g$ for 5 min, $2000 \times g$ for 10 min, and $10,000 \times g$ for 30 min to remove cellular debris at 4°C. Debris-free media was then spun at $100,000 \times g$ for 2 h at 4°C. The supernatant was saved as the nonexosomal fraction. The pellet was resuspended in PBS and then spun again at $100,000 \times g$ for 80 min at 4°C. The pellet was resuspended in PBS with protease inhibitors.

Iodixanol gradient. A discontinuous gradient from 50% to 10% of OptiPrep (Axis Shield) was used to fractionate exosome pellets. The exosome pellet was resuspended in 200 μl 50% OptiPrep and step-gradients of OptiPrep decreasing 10% with each step were carefully layered on top. The step-gradient was centrifuged at $110,000 \times g$ for 16 h at 4°C. Fractions of 110 μl were carefully removed from the top down, diluted with PBS to 1 ml, and centrifuged at $110,000 \times g$ for 1 h to repellet exosomes. The pellets were resuspended in PBS and analyzed by Western blot.

Nanosight. The size and concentration of exosomes was determined on a NanoSight NS300 (Malvern Instruments). Following isolation by ul-

Table 1. List of primary antibodies used for immunostaining, immunoprecipitation, or Western blot studies

Primary antibodies	Source	Identifier
Mouse monoclonal anti-14-3-3θ	Abcam	Catalog #ab10439 AB_297180
Mouse monoclonal anti-pan 14-3-3s	Santa Cruz Biotechnology	Catalog #sc1657 AB_626618
Mouse monoclonal anti-α-synuclein	BD Biosciences	Catalog #610787 AB_398108
Rabbit polyclonal anti-α-synuclein	Cell Signaling Technologies	Catalog #2642S AB_10695412
Mouse monoclonal anti-phospho-S129 α-synuclein	BioLegend	Catalog #825701 AB_2564891
Rabbit polyclonal anti-phospho-S129 α-synuclein	Abcam	Catalog #ab168381
Rabbit monoclonal anti-phospho-S129 α-synuclein	Abcam	Catalog #ab51253 AB_869973
Mouse monoclonal anti-flotillin 1	BD Biosciences	Catalog #610820 AB_398139
Rabbit monoclonal antibody against GFP	Cell Signaling Technologies	Catalog #2956S AB_1196615
Mouse monoclonal antibody against HA	Covance	Catalog #MMS-101P AB_2314672
Mouse monoclonal antibody against V5	ThermoFisher	Catalog #R960-25 AB_2556564
Mouse monoclonal antibody against α-tubulin	Sigma-Aldrich	Catalog #T9026 AB_477593

tracentrifugation, exosome pellets were resuspended in 60 μl cold PBS with repeated pipetting and vortexed for 10 s. Then 15 μl of the exosome suspension was diluted to a total volume of 1 ml PBS and analyzed on a NanoSight NS300 infused with a syringe pump set at 25 a.u. Data were collected for each sample in 10 repeats of 60 s video and analyzed using NanoSight NTA 3.0 software.

Cryo-EM. For Cryo-EM, 3 μl of exosome sample was applied to glow-discharged 200 mesh Quantifoil R 2/1 grids (Electron Microscopy Sciences) and vitrified in liquid ethane using an FEI Vitrobot Mark IV as previously described (Dearborn et al., 2017). Frozen grids were transferred to a Gatan 622 cryo-holder and observed in an FEI Tecnai F20 electron microscope (FEI) operated at 200 kV. Images were collected under low-dose conditions on a Gatan Ultrascan 4000 CCD camera with magnifications from 38,000–65,500× and 2.0–3.0 μm defocus.

Complementation assay. αSyn complementation assay was performed as previously described (Danzer et al., 2011). Briefly, H4 neuroglioma cells were cotransfected with αsyn-hGLuc1 (S1), αsyn-hGLuc2 (S2), and either empty vector, 14-3-3θ, difopein-eYFP, or mutant difopein-eYFP using SuperFect transfection reagent (Qiagen). Cells were incubated in serum-free and phenol red-free OptiMEM media. At 48 h after transfection, CM was spun at $3000 \times g$ for 5 min to remove cellular debris and then was transferred to a separate 96-well plate. Luciferase activity was measured at 480 nm using a Synergy 2 plate reader (BioTek) following addition of 40 μM coelenterazine.

Size exclusion chromatography. For analytical size exclusion chromatography (SEC) of αsyn, CM from induced isyn cells was diluted in 1× PBS, pH 6.8, to 4 mg/ml. 20 μl (80 μg) was then loaded onto a NGC FPLC (Bio-Rad Laboratories), injected on a Yarra 3 μm SEC-2000 column (300 × 7.8 mm, Phenomenex), and run at 0.7 ml/min in 1× PBS, pH 6.8. Fractions (250 μl) were collected from elution volume 4–12.5 ml. This corresponds to the end of the void volume, as determined by a Blue Dextran standard, and the buffer front, as determined by imidazole elution. After SEC, αsyn in 50 μl of each fraction was measured using an ELISA for αsyn.

Protein misfolding cyclic amplification of αsyn. Recombinant human αsyn was purified according to the method previously published (Volpicelli-Daley et al., 2014). Upon thawing, purified αsyn protein was centrifuged at $100,000 \times g$ for 30 min at 4°C to remove any aggregates that may have formed during the freeze-thaw process. Monomer αsyn was then diluted to 50 μM concentration in 10 mM Tris, pH 7.6, with 150 mM NaCl in 0.2 ml PCR tubes with zirconium oxide beads. Twenty-five microliters of culture media from various cells were added to each PMCA reaction. PCR tubes were then placed in Q700 sonicator (Qsonica) where they received repeated cycles of 10 s sonication, followed by 30 min incubation at 37°C. Thioflavin T (ThT) readings were performed at various time points by transferring 2 μl of sample into wells of a black
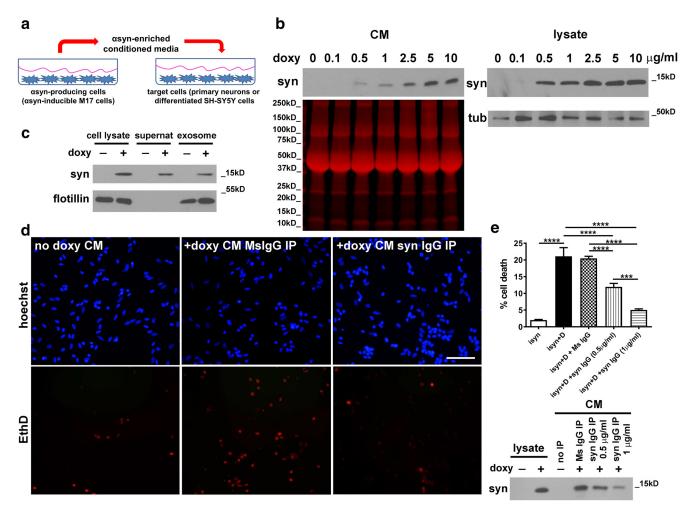
Figure 1. Paracrine αsyn model. ***a***, Schematic of isyn cell model. In response to doxycycline treatment, doxy-inducible αsyn cells produce an excess of αsyn that is released into the CM. When transferred to separately cultures neurons, αsyn-enriched CM induces neuronal death. ***b***, Doxy dose–response. Increasing doxy concentrations induced higher amounts of αsyn in the cell lysates of isyn cells, and, correspondingly, higher amounts of αsyn is released into the CM. Equal protein levels were loaded for each CM sample. Coomassie stain confirmed equal protein loading for the CM. ***c***, αSyn that is released in response to αsyn induction is found in both the exosomal and non-exosomal fractions of CM after high-speed ultracentrifugation of the CM. ***d***, CM from doxy-induced isyn induces cell death in differentiated SH-SY5Y cells that are separately cultured. Representative images of differentiated SH-SY5Y cells treated with CM from uninduced or induced isyn cells. Ethidium D labels nuclei of dying cells, while Hoechst 33342 stains the nuclei of all cells. Scale bar, 100 μm. ***e***, Immunoprecipitation of αsyn from CM by αsyn-directed monoclonal antibody reduces the toxicity of the CM in a dose-dependent manner. Quantification of cell death in differentiated SH-SH5Y cells treated with CM from induced isyn cells in which αsyn was immunodepleted. Western blot of CM after immunoprecipitation confirms reduction of αsyn from the CM. $n = 3$–5 per condition. $***p = 0.0005$, $****p < 0.0001$ (Tukey's multiple-comparison test). Error bars represent SEM. D, Doxy.

bottomed 96-well plate, and incubating with 198 μl 20 μM ThT solution (20 μM ThT, 50 mM glycine, pH 8.5) for 5 min. ThT fluorescence readings were performed on a Tecan M200 plate reader with an excitation of 440 nm and an emission of 480 nm.

αSyn fibril preparation. Fibrils were generated by incubating purified monomeric αsyn at a concentration of 5 mg/ml in 50 mM Tris, pH 7.5, with 166 mM KCl with constant agitation at 700 rpm at 37°C for 7 d. Before addition to primary neurons, αsyn fibrils were diluted in PBS to 1 mg/ml and then sonicated with a 1/8 inch probe tip sonicator (Fisher Scientific, model 120) for 65 pulses over 40 s at power level 2. Sonicated αsyn fibrils were added to primary neuronal cultures at 0.5 or 1 μg/ml in neuronal media.

Microfluidic chambers. Primary neurons were plated in microfluidic chambers with three cell compartments (TCND1000, Xona Microfluidics) per the manufacturer's instructions. At 5 DIV, PBS or PFFs were added to Chamber 1 only. A 75 μl difference in media volume was maintained between each chamber with the lowest volume in Chamber 1 to control the direction of media flow.

Immunocytochemistry. Primary neurons were fixed in 4% paraformaldehyde with 4% sucrose and 1% Triton X-100 for 15 min. After washing in PBS, neurons were permeabilized with 3% BSA and 0.1% Triton X-100 in PBS for 10 min and then blocked with 3% BSA in PBS for 20 min. Neurons were incubated overnight with pS129-αsyn antibody (Abcam, ab51253) in 3% BSA. After washing, neurons were incubated with goat anti-rabbit or anti-mouse secondary antibody in 3% BSA. Neurons were imaged using an Olympus BX51 epifluorescence microscope. Ten high-power (20×) fields per well were randomly selected for quantification, and the percentage of area positive for pS129-αsyn immunoreactivity was quantitated using ImageJ with the rater blind to experimental conditions (Schneider et al., 2012). For triple-chamber slides, images of the whole chamber were taken for quantification of pS129-αsyn immunoreactivity.

Experimental design and statistical analysis. GraphPad Prism 7 was used for statistical analysis of experiments. Data were analyzed by either Student's t test or by one-way or two-way ANOVA, followed by *post hoc* pairwise comparisons using Sidak's or Tukey's multiple-comparison tests. Figures 1e, 2b–f, 3b–e, 4b,c,f,h,i, 5b–f, 6f, and 9a,b use one-way ANOVA followed by *post hoc* Tukey's multiple-comparison test if necessary. Figures 4d,e,k, 10b,c, 11b,c, and 12b,c use two-way ANOVA followed by *post hoc* Sidak's multiple-comparison test. Figures 6c–e, 7a,c, 8b,d,e,f, 11e, and 12e use unpaired Student's t test. Statistical significance was set at $p \leq 0.05$.

For Figures 13*c,d*, and 14*b,c*, data were log transformed before unpaired Student's *t* test with correction for multiple comparisons using the Holm–Sidak method.

All the details of experiments can be found in Results or the figure legends. All data values are presented as mean ± SEM. ANOVA related statistics (*F* statistic, *p* values) are noted in the results section, whereas the *post hoc* test results are found in the figure legends. For *t* tests, the *t* statistic and *p* values are noted in Results.

Results

14-3-3θ reduces toxicity of released αsyn in a non-cell autonomous manner

We have developed a paracrine αsyn model to evaluate the toxicity associated with neuronally-released αsyn (Fig. 1). We created a doxy-inducible neuroblastoma line, termed isyn, which upon doxy treatment releases αsyn into the CM (Fig. 1*a*). This paracrine system is similar to those developed by other groups in which αsyn overexpression in neuronal lines promotes αsyn release into the conditioned media with resultant toxicity to neighboring neurons (Desplats et al., 2009; Emmanouilidou et al., 2010; Danzer et al., 2011). Induction of αsyn expression with doxy in isyn cells led to the detection of αsyn in the CM in a dose-dependent manner (Fig. 1*b*). Previous research has shown that αsyn is released through exosomal and non-exosomal pathways (Lee et al., 2005; Liu et al., 2009; Emmanouilidou et al., 2010; Hasegawa et al., 2011; Danzer et al., 2012). We fractionated the CM into exosomal and non-exosomal fractions by sequential, high ultracentrifugation techniques (Thery et al., 2006) and found that αSyn was released into both exosomal and non-exosomal fractions (Fig. 1*c*). This neuronally-released αsyn is toxic to separately cultured neurons: transfer of αsyn-enriched CM from induced isyn cells induces cell death of separately cultured differentiated SH-SY5Y neuroblastoma cells and primary neurons (Fig. 1*d*). Toxicity from αsyn-enriched CM depends on αsyn, as immunodepletion of αsyn from the CM eliminated toxicity in a dose-dependent manner (Fig. 1*d,e*; one-way ANOVA, $F_{(4,15)} = 96.84$, $p < 0.0001$).

We tested whether 14-3-3 proteins could affect the toxicity of released αsyn. Isyn cells were transduced with a V5-tagged 14-3-3θ doxy-inducible lentivirus and selected for polyclonal stable transfection. Toxicity of αsyn-enriched CM was reduced to basal levels when 14-3-3θ was co-overexpressed with αsyn upon doxy induction in isyn cells. Separately-cultured primary hippocampal neurons showed 31% cell death at 24 h when treated with CM from induced isyn cells, but toxicity was back to baseline when treated with CM from induced 14-3-3θ-overexpressing isyn cells (Fig. 2*a,b*; one-way ANOVA: $F_{(3,18)} = 43.81$, $p < 0.0001$). Similarly, 14-3-3θ overexpression in isyn cells also reduced the toxicity of αsyn-enriched CM that was transferred to cortical neurons (Fig. 2*c*; one-way ANOVA: $F_{(3,12)} = 202.7$, $p < 0.0001$) or differentiated SH-SY5Y cells (Fig. 2*d*; one-way ANOVA: $F_{(2,9)} = 348.3$, $p < 0.0001$) back to baseline. Cellular αsyn levels in isyn cells were not reduced but slightly increased with 14-3-3θ overexpression (see Fig. 4*c*; one-way ANOVA: $F_{(3,20)} = 259$, $p < 0.0001$).

We next tested whether the overexpression of 14-3-3θ in target neurons impacted the toxicity of CM from induced isyn cells. Hippocampal neurons cultured from 14-3-3θ transgenic mice were resistant to αsyn-enriched CM toxicity compared with neurons cultured from nontransgenic littermates (Fig. 2*e*; one-way ANOVA, $F_{(3,44)} = 8.242$, $p = 0.0002$).

We next examined whether the protective effects of 14-3-3θ against the toxicity of released αsyn was specific to 14-3-3θ or whether other 14-3-3 isoforms could be protective. Isyn cells were transduced with a V5-tagged 14-3-3ζ doxy-inducible lenti-

virus and selected for polyclonal stable transfection. Toxicity of αsyn-enriched CM was minimally reduced when 14-3-3ζ was co-overexpressed with αsyn upon doxy induction in isyn cells (Fig. 2*f*; one-way ANOVA, $F_{(5,30)} = 407.3$, $p < 0.0001$).

14-3-3 proteins have been shown to promote cell survival (Porter et al., 2006), and we previously demonstrated that 14-3-3θ overexpression reduces cell death in neurotoxin and mutant LRRK2 models in a cell autonomous manner (Yacoubian et al., 2010; Slone et al., 2011, 2015; Ding et al., 2015; Lavalley et al., 2016). We hypothesized that protection against αsyn-enriched CM when 14-3-3θ was overexpressed in isyn cells could be mediated by the transfer of exogenous V5-tagged 14-3-3θ into the target neurons exposed to the CM. Exogenous V5-tagged 14-3-3θ could not be detected by Western blot or immunocytochemistry in differentiated SH-SY5Y cells exposed to CM from 14-3-3θ-overexpressing isyn cells (Fig. 2*g,h*). We conclude that the protective effect of 14-3-3θ when overexpressed in isyn cells is not likely due to the transfer of exogenous V5-tagged 14-3-3θ into target neurons.

14-3-3 inhibition increases the toxicity of released αsyn

We next tested whether inhibition of endogenous 14-3-3s would impact the toxicity of neuronally-released αsyn. Difopein (dimeric 14-3-3 peptide inhibitor) is a high-affinity 14-3-3 competitive antagonist peptide that disrupts 14-3-3/ligand interactions by binding within the amphipathic groove of 14-3-3s without selectivity among the different isoforms (Masters and Fu, 2001). Mutant difopein is a control peptide with two amino acid mutations that prevents the difopein peptide from binding 14-3-3s (Masters and Fu, 2001). iSyn cells were transduced with a doxy-inducible difopein tagged with eYFP lentivirus (isyn/dif) or with a doxy-inducible mutant difopein tagged with eYFP lentivirus (isyn/yfp). Difopein-eYFP increased toxicity by twofold in primary hippocampal neurons at 24 h after treatment with αsyn-enriched CM compared with mutant difopein-eYFP control (Fig. 3*a,b*; one-way ANOVA: $F_{(3,26)} = 72.27$, $p < 0.0001$). Similarly, difopein-eYFP increased toxicity to 45.9% in differentiated SH-SY5H cells at 48 h after treatment with αsyn-enriched CM (Fig. 3*c*; one-way ANOVA: $F_{(3,12)} = 42.68$, $p < 0.0001$). Whereas doxy treatment dramatically increased cellular αsyn levels, difopein expression did not alter intracellular αsyn levels in isyn cells (see Fig. 5*c*; one-way ANOVA: $F_{(3,12)} = 412.4$, $p < 0.0001$).

To confirm whether CM toxicity was still secondary to αsyn released in the CM when difopein was coexpressed, we immunoprecipitated αsyn from the CM of difopein-eYFP and mutant difopein-eYFP (control) expressing isyn cells using an αsyn-specific antibody before transfer of the CM to differentiated SH-SY5Y cells (Fig. 3*d*). Toxicity of CM from difopein-eYFP or mutant difopein-eYFP isyn cells was eliminated by αsyn immunoprecipitation (Fig. 3*d*; one-way ANOVA: $F_{(5,30)} = 71.23$, $p < 0.0001$). This finding suggests that the enhanced toxicity of CM from difopein-expressing isyn cells was due to αsyn and not due to the release of other factors that may promote toxicity.

To test whether specific inhibition of endogenous 14-3-3θ was sufficient to reduce αsyn release, we used a shRNA targeting 14-3-3θ to knockdown 14-3-3θ expression in isyn cells. CM from isyn cells in which 14-3-3θ expression was reduced (isyn/1433KD cells) induced a 2.7-fold increase in cell death compared with that of isyn cells transfected with control shRNA (isyn/plko cells; Fig. 3*e*; one-way ANOVA: $F_{(5,30)} = 99.77$, $p < 0.0001$).
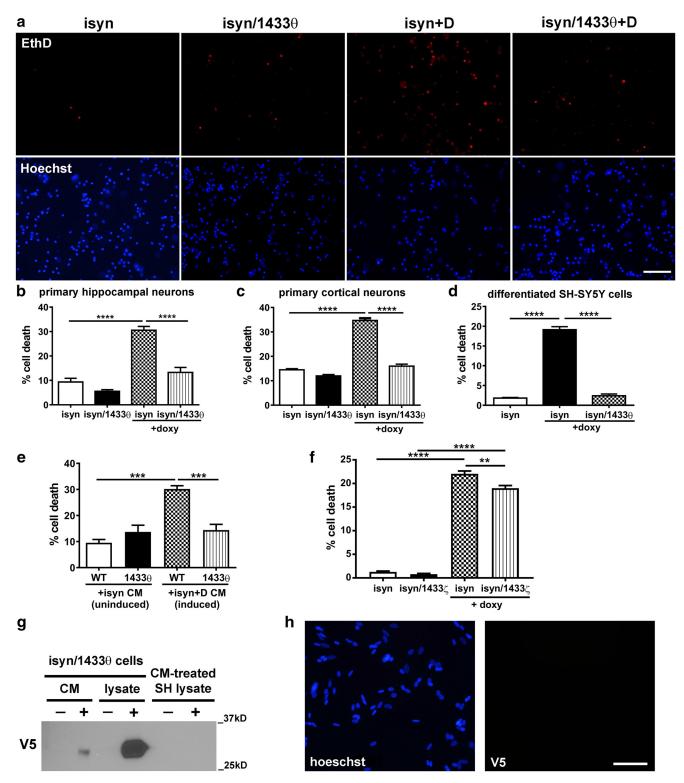
Figure 2. 14-3-3θ overexpression in isyn cells reduces the toxicity of αsyn-enriched CM. **a**, Representative images of primary hippocampal neurons treated with CM from isyn cells or isyn cells expressing an inducible 14-3-3θ construct. Ethidium D labels the nuclei of dying cells, whereas Hoechst 33342 stains the nuclei of all cells. Scale bar, 100 μm. **b**, Quantification of cell death in primary hippocampal neurons treated with CM from isyn or isyn/14-3-3θ cells for 24 h. $n = 3$ independent rounds with two replicates per round. **c**, Quantification of cell death in primary cortical neurons treated with CM from isyn or isyn/14-3-3θ cells for 24 h. $n = 4$. **d**, Quantification of cell death in differentiated SH-SY5Y cells treated with CM from isyn or isyn/14-3-3θ cells at 48 h. $n = 3$ independent rounds with one to two replicates per round. **e**, Overexpression of 14-3-3θ in target primary neurons also reduces toxicity of induced CM from isyn cells. Quantification of cell death in primary hippocampal neurons from nontransgenic or 14-3-3θ transgenic mice treated with CM from isyn cells at 24 h. $n = 4$ independent rounds with one to six replicates/round. **f**, Quantification of cell death in differentiated SH-SY5Y cells treated with CM from isyn or isyn/14-3-3ζ cells at 48 h. $n = 3$ independent rounds with two replicates per round. **g**, Western blot of cell lysates from differentiated SH-SY5Y cells treated with CM from induced isyn/14-3-3θ cells. Although the V5 tag of exogenous 14-3-3θ is detected in lysates from induced isyn/14-3-3θ cells and in the CM, V5 is not detected in lysates from differentiated SH-SY5Y cells treated with CM. **h**, Exogenous V5-tagged 14-3-3θ is not transferred to target neurons exposed to CM from isyn/14-3-3θ cells. Immunocytochemistry for V5 tag in differentiated SH-SY5Y cells treated with CM from isyn/14-3-3θ cells with or without induction. $**p < 0.01$, $***p < 0.001$, $****p < 0.0001$ (Tukey's multiple-comparison test). Error bars represent SEM. D, Doxy.
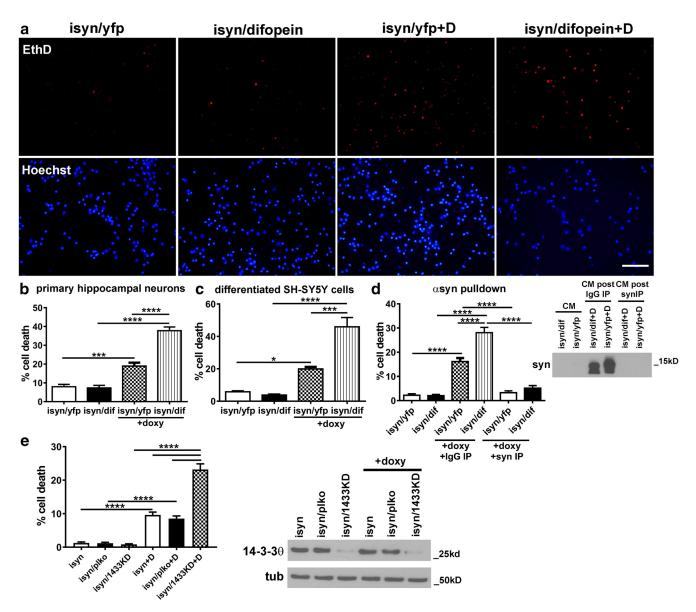
Figure 3. 14-3-3 inhibition in isyn cells increases the toxicity of αsyn-enriched CM. **a**, Representative images of primary hippocampal neurons treated with CM from isyn cells expressing either an inducible difopein-eYFP (isyn/dif) construct or an inducible mutant difopein-eYFP construct (isyn/yfp; control). Scale bar, 100 μm. **b**, Quantification of cell death in primary hippocampal neurons treated with CM from isyn/ difopein-eYFP cells (isyn/dif) or control isyn/mutant difopein-eYFP (isyn/yfp) cells at 24 h. $n =$ three independent rounds with two to three replicates per round. **c**, Quantification of cell death in differentiated SH-SY5Y cells treated with CM from isyn/ difopein-eYFP cells (isyn/dif) or control isyn/mutant difopein-eYFP (isyn/yfp) cells at 48 h. $n =$ 4 independent rounds with one replicate per round. **d**, Immunoprecipitation of αsyn from CM by αsyn-directed monoclonal antibody eliminates the toxicity of CM from induced control isyn/mutant difopein-eYFP (isyn/yfp) cells and from induced isyn/difopein-eYFP (isyn/dif) cells. Quantification of cell death in differentiated SH-SY5Y cells treated with CM from isyn/dif or control isyn/yfp cells with or without αsyn immunodepletion. Western blot of CM after αsyn immunoprecipitation confirms that αsyn is eliminated from the CM. $n =$ 4 rounds with one to two replicates/round. **e**, Quantification of cell death in differentiated SH-SY5Y cells treated with CM from isyn cells (isyn), control isyn/plko.1 empty vector cells (isyn/plko), or isyn/14-3-3θ shRNA (isyn/14-3-3 KD) cells at 48 h. $n =$ 3 independent rounds with two replicates per round. Western blot of cell lysates confirms 14-3-3θ protein levels are reduced in isyn/14-3-3 KD cells. $*p < 0.05$, $***p < 0.001$, $****p < 0.0001$ (Tukey's multiple-comparison test). Error bars represent SEM. D, Doxy.

Overexpression of 14-3-3θ induces αsyn release

As 14-3-3θ reduced the toxicity of αsyn released by isyn cells, we next examined whether 14-3-3θ regulated the amount of αsyn released in this paracrine model system. Surprisingly, when both αsyn and 14-3-3θ overexpression were induced by 10 μg/ml doxy, we observed a 2.6-fold increase in the amount of αsyn released into the CM as measured by Western blot (Fig. 4a–c; one-way ANOVA: $F_{(3,24)} = 61.91, p < 0.0001$). To control for any potential differences between αsyn expression in the cell lysates, we also normalized αsyn in the CM to αsyn expression in the cell lysates and still observed a 2.1-fold increase in αsyn release (unpaired, two-tailed Student's t test: $t_{(10)} = 5.796, p = 0.0002$).

14-3-3θ overexpression promoted higher levels of αsyn release into the CM compared with control at multiple doses of doxy induction (Fig. 4d; two-way ANOVA, treatment: $F_{(1,24)} = 34.58$, $p < 0.0001$; dose: $F_{(5,24)} = 29.23; p < 0.0001$; interaction: $F_{(5,24)} = 3.584 \, p = 0.0146$).

To test whether αsyn release induced by 14-3-3θ changed over time, we measured αsyn release into the CM at 2, 3, 4, and 7 d after 10 μg/ml doxy induction by ELISA. A difference in total αsyn release was noted as early as at 3 d but became statistically significant at 4 and 7 d after treatment (Fig. 4e; two-way ANOVA, treatment: $F_{(1,16)} = 471.6, p < 0.0001$; time: $F_{(4,16)} = 1751, p < 0.0001$; interaction: $F_{(4,16)} = 454.4, p <$
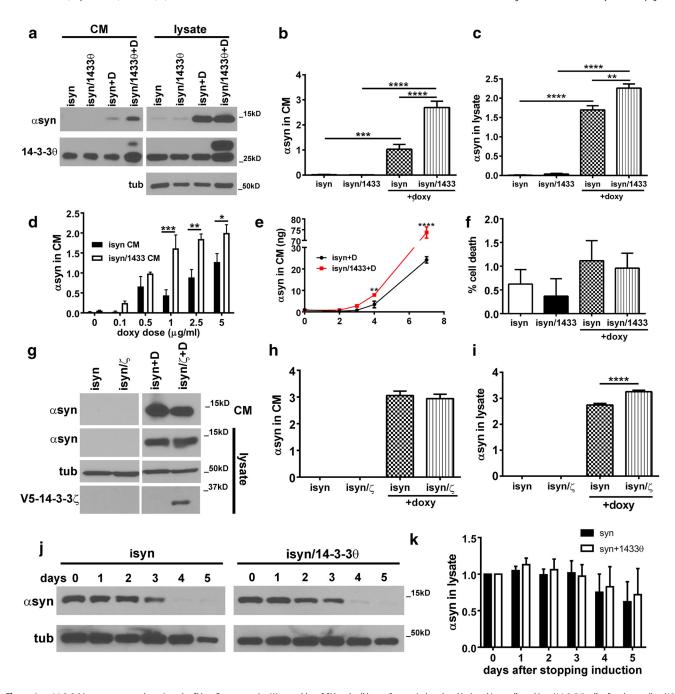
Figure 4. 14-3-3θ increases αsyn release into the CM. ***a***, Representative Western blot of CM and cell lysate from uninduced and induced isyn cells and isyn/14-3-3θ cells after doxycycline (10 μg/ml) induction for 96 h. Equal protein levels were loaded for each CM sample. ***b***, Quantification of αsyn in the CM from isyn and isyn/14-3-3θ cells with and without 96 h induction by Western blot. Equal protein amounts were loaded for each CM sample. $n = 5$ independent rounds with 1–2 replicates per round. ***c***, Quantification of αsyn in the cell lysates from isyn and isyn/14-3-3θ cells with and without 96 h induction by Western blot. αSyn in lysates was normalized to tubulin. $n = 5$ independent rounds with one to two replicates per round. ***d***, Quantification of αsyn in the CM from isyn and isyn/14-3-3θ cells treated with increasing doses of doxy for 96 h by Western blot. Equal protein amounts were loaded for each CM sample. $n = 3$ independent rounds. ***e***, Quantification of αsyn in the CM from isyn and isyn/14-3-3θ cells by ELISA at 2, 3, 4, and 7 d after induction. Equal protein amounts were loaded for each CM sample. $n = 3$ independent rounds with two replicates per round. ***f***, Quantification of cell death in isyn and isyn/14-3-3θ cells with and without induction. Number of Ethidium D-positive cells is normalized to total cell count, as determined by Hoechst 33342 staining. $n = 3$ independent rounds. ***g***, 14-3-3ζ does not alter αsyn release. Representative Western blot of CM and cell lysate from uninduced and induced isyn cells and isyn/14-3-3ζ cells after doxycycline (10 μg/ml) induction for 96 h. ***h***, Quantification of αsyn in the CM from isyn and isyn/14-3-3ζ cells with and without 96 h induction by Western blot. Equal protein amounts were loaded for each CM sample. $n = 4$ independent rounds. ***i***, Quantification of αsyn in the cell lysates from isyn and isyn/14-3-3ζ cells with and without 96 h induction by Western blot. αSyn was normalized to tubulin. $n = 4$ independent rounds. ***j***, ***k***, 14-3-3θ does not alter αsyn clearance. αSyn levels in cell lysates after withdrawal of doxycycline after 3 d of induction. Representative Western blot (j) and quantification (k) of αsyn in cell lysates from isyn and isyn/14-3-3θ cells each day after withdrawal of doxycycline. αSyn was normalized to tubulin. *$p < 0.05$, **$p < 0.01$, ***$p < 0.001$, ****$p < 0.0001$ (Tukey's multiple-comparison test). Error bars represent SEM. D, Doxy.

0.0001). The difference in αsyn release was maintained over time with 14-3-3θ overexpression. Differences in release were not due to cell death, as cell death was limited to ∼1% in induced isyn cells with and without 14-3-3θ overexpression

(Fig. 4f; one-way ANOVA: $F_{(3,8)} = 0.8929$, $p = 0.4854$). Based on these data, we conclude that the ability of 14-3-3θ to reduce the toxicity of αsyn-enriched CM was not secondary to a reduction in the total amount of αsyn released.
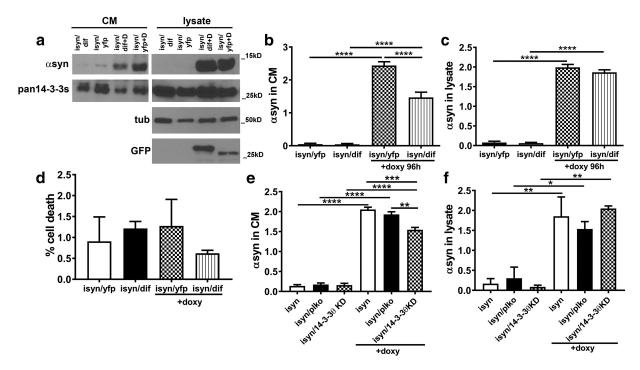
Figure 5. 14-3-3 inhibition reduces αsyn release into the CM. **a**, Representative Western blot of CM and cell lysate from uninduced and induced isyn/difopein-eYFP (isyn/dif) cells and control isyn/mutant difopein-eYFP (isyn/yfp) cells after doxy (10 μg/ml) induction for 96 h. Equal protein levels were loaded for each CM sample. **b**, Quantification of αsyn in the CM from isyn/difopein-eYFP (isyn/dif) cells and control isyn/mutant difopein-eYFP (isyn/yfp) cells with and without 96 h induction by Western blot. Equal protein amounts were loaded for each CM sample. $n = 4$ independent rounds. **c**, Quantification of αsyn in the cell lysates from isyn/difopein-eYFP (isyn/dif) cells and control isyn/mutant difopein-eYFP (isyn/yfp) cells with and without 96 h induction by Western blot. αSyn in lysates was normalized to tubulin. $n = 4$ independent rounds. **d**, Quantification of cell death in isyn/difopein-eYFP (isyn/dif) and control isyn/mutant difopein-eYFP (isyn/yfp) cells with and without induction. $n = 3$ independent rounds. **e**, Quantification of αsyn in the CM from isyn cells and isyn cells transfected with either plko.1 empty vector control lentivirus or 14-3-3θ shRNA lentivirus with and without 96 h induction by Western blot. Equal protein amounts were loaded for each CM sample. $n = 3$ independent rounds. **f**, Quantification of αsyn in the cell lysates from isyn cells and isyn cells transfected with either plko.1 empty vector control lentivirus or 14-3-3θ shRNA lentivirus with and without 96 h induction by Western blot. αSyn in lysates was normalized to tubulin. $n = 3$ independent rounds. *$p < 0.05$, **$p < 0.01$, ***$p < 0.001$, ****$p < 0.0001$ (Tukey's multiple-comparison test). Error bars represent SEM. D, Doxy.

We next examined whether another 14-3-3 isoform affected αsyn release in a similar manner. Isyn cells were transduced with a doxy-inducible 14-3-3ζ lentivirus and then selected for polyclonal stable transfection by hygromycin. While induction of αsyn by doxy promoted αsyn release, no change in the amount of released αsyn was noted in isyn cells also overexpressing 14-3-3ζ compared with isyn cells (Fig. 4g–i; one-way ANOVA, $F_{(3,12)} = 228.8$, $p < 0.0001$).

14-3-3θ overexpression does not alter αsyn clearance

Inhibition of the autophagy-lysosomal pathway increases αsyn release from neurons (Emmanouilidou et al., 2010; Jang et al., 2010; Alvarez-Erviti et al., 2011; Danzer et al., 2012; Lee et al., 2013). We tested whether 14-3-3θ overexpression reduced clearance of αsyn which then indirectly increased αsyn release. iSyn cells with and without 14-3-3θ overexpression were induced with doxy for 4 d for maximal induction and then switched to doxy-free culture media up to another 5 d. Lysates from isyn cells were then collected and probed for αsyn by Western blot. In the absence of doxy, isyn cells slowly reduced αsyn levels near baseline levels over 5 d. We observed no differences in the rate of decline of total intracellular αsyn levels from isyn cells with or without 14-3-3θ overexpression (Fig. 4j,k; two-way ANOVA, treatment: $F_{(1,34)} = 0.2133$, $p = 0.6472$; time: $F_{(5,34)} = 1.547$, $p = 0.2017$; interaction: $F_{(5,34)} = 0.05065$; $p = 0.9983$). This finding suggests that 14-3-3θ in isyn cells does not promote αsyn release by slowing the clearance of αsyn.

Inhibition of 14-3-3s reduces αsyn release

We next tested whether inhibition of endogenous 14-3-3s would impact αsyn release. αSyn released into the CM was reduced in isyn cells expressing the pan 14-3-3 inhibitor difopein-eYFP by ∼40% compared with control isyn cells expressing mutant difopein-eYFP (Fig. 5a–c; one-way ANOVA: $F_{(3,12)} = 136.4$, $p < 0.0001$). While total αsyn levels were dramatically increased with doxy induction, there was no difference in the cell lysates between induced isyn cells expressing difopein-eYFP or mutant difopein-eYFP (Fig. 5c; one-way ANOVA: $F_{(3,12)} = 412.4$, $p < 0.0001$). Cell death in isyn cells expressing either difopein-eYFP or mutant difopein-eYFP was only 1% (Fig. 5d; one-way ANOVA: $F_{(3,8)} = 0.4744$, $p = 0.7087$), such that cell death was not the cause of differences in αsyn release.

To test whether specific inhibition of endogenous 14-3-3θ was sufficient to reduce αsyn release, we tested the effect of a shRNA targeting 14-3-3θ in isyn cells. 14-3-3θ knockdown caused a reduction in the total amount of αsyn released (Fig. 5e; one-way ANOVA: $F_{(5,12)} = 317$, $p < 0.0001$). αSyn levels in cell lysates were increased upon doxy treatment in control shRNA and 14-3-3θ shRNA transduced isyn cells, but there was no difference in cellular αsyn levels between the different lines (Fig. 5f; one-way ANOVA: $F_{(5,12)} = 13.47$, $p = 0.0001$).

14-3-3θ overexpression increases αsyn release through exosomal and non-exosomal pathways

Based on our release data, the protective effect of 14-3-3θ on the toxicity of neuronally-released αsyn is not secondary to a reduc-

tion in the total amount of αsyn released into the CM. Previous research has shown that αsyn is released through exosomal and non-exosomal pathways, and certain studies have suggested that exosomally-released αsyn may have increased toxic potential (Lee et al., 2005; Liu et al., 2009; Emmanouilidou et al., 2010; Hasegawa et al., 2011; Danzer et al., 2012; Stuendl et al., 2016; Ngolab et al., 2017). We fractionated the CM into exosomal and non-exosomal fractions by sequential, high ultracentrifugation techniques (Thery et al., 2006) to test whether 14-3-3θ possibly preferentially directed release through non-exosomal pathways. To rule out the possibility that αsyn that precipitated with exosomal pellets were not just large aggregates unassociated with exosomes that spun down due to high centrifugation speeds, we layered exosomal pellets after ultracentrifugation onto a discontinuous iodixanol gradient followed by ultracentrifugation at 250,000 × g for 2 h. αSyn was found only in the fractions that were positive for the exosomal marker flotillin (Fig. 6a). This confirmed that αsyn that precipitated into the exosomal pellets was indeed associated with the exosomes. Cryo-EM and nanosight analysis revealed nanometer-sized vesicles consistent with exosomes (Fig. 6b,e).

The vast majority of released αsyn in our model was associated with the non-exosomal fraction from isyn cells. Only ~0.6% of total αsyn was associated with the exosomal fraction. When 14-3-3θ was overexpressed in isyn cells, the amount of αsyn released in the exosomal fraction was increased nearly twofold (Fig. 6c; unpaired, two-tailed t test: $t_{(6)} = 4.306$, $p = 0.0051$). αSyn released in the non-exosomal fraction was also increased by 14-3-3θ overexpression (Fig. 6c; unpaired, two-tailed t test: $t_{(6)} = 4.742$, $p = 0.0032$). Conversely, we also examined the effect of 14-3-3 inhibition by difopein on exosomal and non-exosomal αsyn release. When isyn cells expressed the 14-3-3 inhibitor difopein-eYFP, αsyn release was reduced in both the exosomal (unpaired, two-tailed t test: $t_{(4)} = 7.246$, $p = 0.0019$) and non-exosomal fractions (unpaired, two-tailed t test: $t_{(4)} = 4.877$, $p = 0.0082$) compared with isyn cells expressing mutant difopein-eYFP (Fig. 6d). Thus, the total change in αsyn release induced by 14-3-3 manipulation occurred through both exosomal and non-exosomal pathways, and 14-3-3s did not lead to preferential release from one pathway versus the other.

We have previously shown that 14-3-3s increase the release of LRRK2 into exosomes (Fraser et al., 2013). To examine whether 14-3-3θ overexpression could promote exosomal release in general, we used Nanosight analysis to determine the amount of exosomes released (Fig. 6e). We observed no difference in total exosomal counts between doxy-induced isyn cells or isyn/14-3-3θ cells (Fig. 6e: unpaired, two-tailed t test: $t_{(10)} = 0.7024$, $p = 0.4984$). Similarly, exosomal counts from induced isyn/difopein-eYFP cells were similar to that from isyn/mutant difopein-eYFP control cells (Fig. 6e; unpaired, two-tailed t test: $t_{(6)} = 0.3996$, $p = 0.7033$).

Exosomal αsyn does not mediate αsyn toxicity in the paracrine system
To determine whether the toxicity of αsyn-enriched CM from isyn cells was mediated by the exosomal and/or non-exosomal fractions, we fractionated the αsyn-enriched CM and then transferred each fraction to target cells to measure toxicity. We found that almost all of the toxicity due to released αsyn was associated with the non-exosomal fraction (Fig. 6f; one-way ANOVA, $F_{(6,35)} = 50.27$, $p < 0.0001$).

14-3-3θ is released into the CM and coimmunoprecipitates with αsyn
We next examined whether 14-3-3θ levels were altered in the CM by 14-3-3 manipulation. Exogenous V5-tagged 14-3-3θ and endogenous 14-3-3θ levels were increased in the CM from isyn cells overexpressing 14-3-3θ compared with control isyn cells (Fig. 7a; unpaired, two-tailed t test: $t_{(14)} = 7.833$, $p < 0.0001$). 14-3-3θ coimmunoprecipitated with αsyn from the CM from induced isyn cells. In the presence of 14-3-3θ overexpression, exogenous V5-tagged 14-3-3θ and higher amounts of endogenous 14-3-3θ coimmunoprecipitated with the released αsyn, whose total levels were increased (Fig. 7b).

In contrast, 14-3-3θ levels in the CM were significantly decreased from isyn cells expressing difopein-YFP compared with isyn cells expressing mutant difopein-YFP (Fig. 7c; unpaired, two-tailed t test: $t_{(4)} = 6.505$, $p = 0.0029$). This finding suggests that 14-3-3 inhibition interfered with the secretion of 14-3-3θ. In addition, less endogenous 14-3-3θ coimmunoprecipitated with αsyn from the CM of isyn cells expressing difopein-eYFP compared with that of isyn cells expressing mutant difopein-eYFP (Fig. 7d).

14-3-3θ regulates αsyn oligomerization
Oligomerization of αsyn is an important feature promoting αsyn toxicity. 14-3-3θ overexpression reduces intracellular αsyn aggregation in H4 neuroglioma cells (Yacoubian et al., 2010), and 14-3-3θ and 14-3-3η reduce recombinant αsyn aggregation as demonstrated by atomic force microscopy (Plotegher et al., 2014). Since αsyn released into the CM was complexed with 14-3-3θ, we hypothesized that 14-3-3θ could impact αsyn oligomerization. We first fractionated CM from induced isyn cells by size exclusion chromatography and observed that the released αsyn from induced isyn cells was primarily eluted in fractions ~7–8.5 ml (Fig. 8a), fractions representing molecular sizes >14 kDa, the expected monomeric αsyn size. Others groups have similarly shown that released αsyn under overexpression conditions is found in higher molecular weight fractions by SEC (Emmanouilidou et al., 2010; Danzer et al., 2011). When 14-3-3θ was overexpressed in isyn cells, the amount of released αsyn found in these higher molecular weight fractions was significantly reduced (Fig. 8a,b; unpaired, two-tailed t test: $t_{(4)} = 3.237$, $p = 0.0318$). This reduction in higher molecular weight αsyn when 14-3-3θ was overexpressed was associated with an increase in αsyn in fractions in which monomeric αsyn is expected (Fig. 8a). ELISA of the total CM before SEC fractionation confirmed that total αsyn levels was overall higher in CM from isyn/14-3-3θ cells compared with that from isyn cells despite the reduction in higher molecular weight αsyn.

In contrast, expression of difopein-eYFP in isyn cells increased the amount of released αsyn in the higher molecular weight fractions compared with that from control isyn cells expressing mutant difopein-eYFP (Fig. 8c,d; unpaired, two-tailed t test: $t_{(4)} = 2.947$, $p = 0.0421$). In addition, there was a relative shift in the size of αsyn released from isyn cells expressing difopein-eYFP toward larger molecular weight size (Fig. 8c). ELISA of total CM before SEC fractionation confirmed that total αsyn levels was overall lower in the CM from difopein-expressing isyn cells compared with that from control cells despite the increase in higher molecular weight αsyn.

While SEC fractionation demonstrated that 14-3-3θ regulates the biochemical and conformational profile of released αsyn, it is unclear whether αsyn eluted in higher molecular weight fractions is truly oligomeric or may instead reflect native αsyn in an ex-
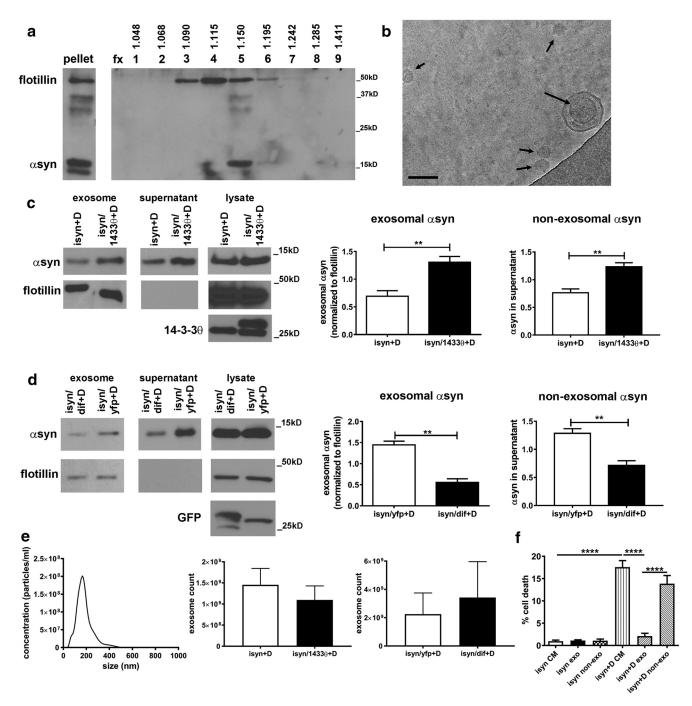
Figure 6. 14-3-3θ regulates αsyn release into both exosomal and non-exosomal fractions. **a**, Exosomal pellet obtained by ultracentrifugation of CM from induced isyn cells was layered onto a discontinuous iodixanol gradient and then underwent ultracentrifugation. αSyn was found only in the fractions that were positive for the exosomal marker flotillin. Density is shown above each fraction. **b**, Cryo-EM of exosomal pellet from induced isyn cells reveals vesicular structures of appropriate diameters for exosomes. Scale bar, 100 nm. **c**, Quantification of αsyn in the exosomal and non-exosomal (supernatant) fractions from isyn and isyn/14-3-3θ cells with and without 96 h induction by Western blot. $n = 4$ independent rounds. Exosomal αsyn was normalized to flotillin. Equal protein amounts were loaded for each supernatant fraction. **$p < 0.01$ (Student's t test). **d**, Quantification of αsyn in the exosomal and non-exosomal (supernatant) fractions from isyn/difopein-eYFP (isyn/dif) and isyn/mutant difopein-eYFP (isyn/yfp) control cells with and without 96 h induction by Western blot. $n = 3$ independent rounds. Exosomal αsyn was normalized to flotillin. Equal protein amounts were loaded for each supernatant fraction. **$p < 0.01$ (Student's t test). **e**, Total exosome counts from exosomal fraction from CM of isyn cells, isyn/14-3-3θ cells, isyn/difopein-eYFP (isyn/dif) cells, and isyn/mutant difopein-eYFP (isyn/yfp) control cells after 96 h of induction with doxycycline. **f**, Quantification of cell death in differentiated SH-SY5Y cells treated with the non-exosomal or exosomal fraction from CM of induced isyn cells. The non-exosomal fraction of the CM from induced isyn cells is toxic to differentiated SH-SY5Y cells, but the exosomal fraction of the CM lacks significant toxicity. $n = 3$ independent rounds with two replicates per round. ****$p < 0.0001$ (Tukey's multiple-comparison test). D, Doxy.

tended conformation, as has been suggested previously (Fauvet et al., 2012; Lashuel et al., 2013). As an alternative measure of the oligomerization of released αsyn, we used a bioluminescent protein-fragment complementation assay in which a luciferase signal is generated when αsyn fused to a non-bioluminescent amino terminal luciferase fragment (S1) interacts with αsyn fused to a carboxy-terminal luciferase fragment (S2; Danzer et al., 2011). The luciferase signal generated by syn-syn interaction is a measure of oligomeric αsyn that falls within the dimer to ~30 mer range (Danzer et al., 2011). Using this assay, we
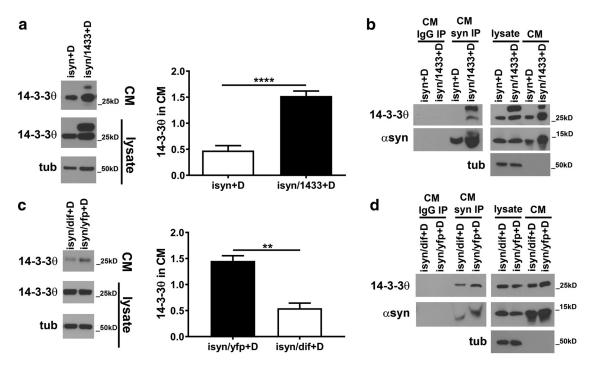
Figure 7. 14-3-3 inhibition reduces 14-3-3θ release and its association with αsyn in CM. ***a***, Quantification of endogenous and exogenous 14-3-3θ released into CM from induced isyn and isyn/14-3-3θ cells. Exogenous V5-tagged 14-3-3θ runs slightly higher than endogenous 14-3-3θ due to the V5-his epitope tag. Equal protein amounts were loaded for each CM sample. $n = 8$ independent rounds. ****$p < 0.0001$ (Student's *t* test). ***b***, Representative blot of coimmunoprecipitation of 14-3-3θ with αsyn from CM from induced isyn cells and from induced isyn/14-3-3θ cells. Similar results were obtained on three additional independent runs. ***c***, Quantification of endogenous 14-3-3θ released into CM from induced isyn/difopein-eYFP (isyn/dif) and isyn/mutant difopein-eYFP (isyn/yfp) control cells. Equal protein amounts were loaded for each CM sample. $n = 3$ independent rounds. **$p = 0.0029$ (Student's *t* test). ***d***, Representative blot of coimmunoprecipitation of 14-3-3θ with αsyn from CM from induced isyn/difopein-eYFP (isyn/dif) and isyn/mutant difopein-eYFP (isyn/yfp) control cells. Similar results were obtained on three additional independent runs. Error bars represent SEM. D, Doxy.

found that 14-3-3θ overexpression significantly reduced the amount of luciferase signal in the CM from H4 cells transfected with S1-syn and S2-syn compared with control (Fig. 8*e*; unpaired, two-tailed *t* test: $t_{(17)} = 4.188$, $p = 0.0006$). Conversely, compared with mutant difopein-eYFP, difopein-eYFP increased the luciferase signal in the CM from H4 cells transfected with S1-syn and S2-syn (Fig. 8*f*; unpaired, two-tailed *t* test: $t_{(16)} = 6.632$, $p < 0.0001$).

14-3-3θ reduces the seeding capability of released αsyn
We next tested whether 14-3-3θ could regulate the seeding potential of αsyn-enriched CM using the PMCA assay. PMCA is a technique initially developed to accelerate amplification of prion protein aggregates and has been adapted for measuring the growth of αsyn aggregates (Herva et al., 2014; Shahnawaz et al., 2017; Becker et al., 2018). In this assay, recombinant αsyn is incubated with minute amounts of potential misfolded αsyn "seeds" in αsyn-enriched CM to induce αsyn polymerization; after a brief period of aggregation, the mixture is sonicated to break down the polymers into smaller sizes to generate more seeds for aggregation. Repeated cycles of sonication and incubation allow for exponential growth of polymers, and fibrillization of protein is measured by ThT fluorescence. We confirmed that CM from induced isyn cells induced fibrillization of recombinant αsyn, while CM from uninduced isyn cells failed to induce significant seeding (Fig. 9*a*). CM from induced isyn cells overexpressing 14-3-3θ showed a significant delay in αsyn fibrillization compared with CM from induced isyn cells (Fig. 9a; one-way ANOVA: $F_{(2,69)} = 18.49$, $p < 0.0001$). This is despite the fact that higher total levels of αsyn are present in the CM from isyn cells overexpressing 14-3-3θ. In contrast, CM from induced isyn cells

expressing difopein-eYFP seeded αsyn fibrillization more quickly than that from induced isyn cells expressing mutant difopein-eYFP control peptide despite the finding that difopein reduces the total amount of αsyn released into the CM (Fig. 9*b*; one-way ANOVA: $F_{(2,69)} = 23.04$, $p < 0.0001$). These findings suggest that endogenous 14-3-3s normally maintain αsyn in a protein conformation that has reduced capability of inducing the misfolding of αsyn molecules. These findings also demonstrate that the protein conformation and not the total amount of αsyn released into the CM is important for inducing fibrillization.

14-3-3θ reduces internalization of released αsyn by primary neurons
Another key feature for αsyn spread is the binding, uptake, and internalization of αsyn by target neurons exposed to released αsyn. We examined whether the number of cells that stained for human αsyn was altered by manipulation of 14-3-3s in isyn cells that release αsyn. To measure the uptake and internalization of released αsyn, we took advantage of the species difference between human αsyn released by the human neuroblastoma line and the endogenous mouse αsyn expressed by primary hippocampal neurons. After treatment of the mouse hippocampal cultures with αsyn-enriched CM, we detected human αsyn expression in mouse neurons using a human-specific αsyn antibody as early as 6 h after treatment. Confocal imaging revealed that human αsyn was internalized into neurons exposed to αsyn-enriched CM (Fig. 10*a*). Interestingly, human αsyn appeared to be localized to the nucleus in neurons exposed to αsyn-enriched CM. The percentage of cells that stained for human αsyn increased with time, with maximal percentage of cells positive for human αsyn noted at 24 h (Fig. 10*b*; two-way ANOVA, time:
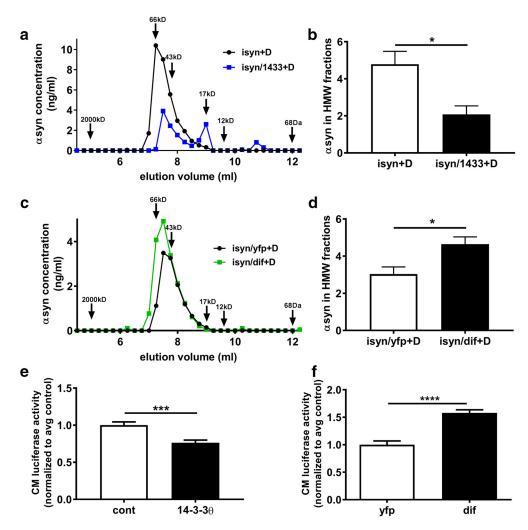
Figure 8. 14-3-3θ reduces oligomerization of released αsyn. **a**, αSyn levels in SEC fractions of CM from induced isyn cells or from induced isyn/14-3-3θ cells. Equal protein amounts (80 μg) per sample were loaded onto the column, and 250 μl fractions were collected from elution volume 4 – 12.5 ml. αSyn in each fraction was measured by ELISA. αSyn from CM from induced isyn cells was primarily found in fractions with molecular weights greater than the expected 14 kDa size of monomeric αsyn, whereas αsyn from CM from induced isyn/14-3-3θ cells was partially shifted into lower molecular weight fractions. Data are representative of three independent experiments. **b**, Quantification of released αsyn detected in high molecular weight (HMW) SEC fractions collected between elution volumes 6 – 8.5 ml. $n = 3$ independent rounds *$p = 0.0318$ (Student's t test). **c**, αSyn levels in SEC fractions of CM from induced isyn/mutant difopein-eYFP (yfp) cells or from induced isyn/difopein-eYFP (dif) cells. Equal protein amounts (80 μg) per sample were loaded onto the column. Data are representative of three independent experiments. **d**, Quantification of released αsyn detected in HMW SEC fractions collected between elution volumes 6 – 8.5 ml. $n = 3$ independent rounds *$p = 0.0421$ (Student's t test). D, Doxy. **e**, Quantification of luciferase activity of CM from H4 neuroglioma cells transfected with S1-syn, S2-syn, and either empty vector (cont) or 14-3-3θ. $n = 4$ rounds with two to three replicates per round. ***$p = 0.0006$ (Student's t test). **f**, Quantification of luciferase activity of CM from H4 neuroglioma cells transfected with S1-syn, S2-syn, and either difopein-eYFP (dif) or mutant difopein-eYFP (yfp). $n = 3$ rounds with three replicates per round. ****$p < 0.0001$ (Student's t test).

$F_{(3,40)} = 22.22$, $p < 0.0001$). In mouse neurons treated with CM from induced isyn cells, we observed 15% of mouse neurons that stained positive for human αsyn at 24 h (Fig. 10b). In contrast, only 7% of mouse neurons stained positive for human αsyn when treated with CM from induced 14-3-3θ-overexpressing isyn cells at 24 h (Fig. 10b; two-way ANOVA, treatment: $F_{(1,40)} = 16.57$, $p = 0.0002$; treatment × time interaction: $F_{(3,40)} = 2.74$, $p = 0.0559$). This reduction in neurons positive for human αsyn was despite the higher amount of total αsyn in the CM from 14-3-3θ-overexpressing isyn cells.

We also tested the impact of 14-3-3 inhibition on αsyn uptake and internalization. The percentage of mouse neurons that were positive for human αsyn at 24 h was increased to 26% when cells were treated with CM from induced isyn/difopein-eYFP cells compared with 14% from induced isyn/mutant difopein-eYFP control cells (Fig. 10c; two-way ANOVA, treatment: $F_{(1,40)} = 14.59$, $p = 0.0005$; time: $F_{(3,40)} = 28.41$, $p < 0.0001$; interaction:

$F_{(3,40)} = 2.46$, $p = 0.0766$). This increase in neurons positive for human αsyn occurs despite the lower amount of total αsyn in the CM from difopein-expressing isyn cells. Although positive staining for human αsyn in mouse neurons points toward uptake and internalization of human αsyn from the CM, this staining could also reflect slowing of the degradation of internalized αsyn in mouse neurons.

14-3-3θ regulates inclusion formation and toxicity in the preformed fibril model

Our studies in the paracrine αsyn model reveals that, despite promoting αsyn release, 14-3-3θ ultimately reduces αsyn transmission and toxicity by reducing αsyn oligomerization, seeding, and internalization by other neurons exposed to released αsyn. We next examined whether 14-3-3θ could impact spread in another αsyn model, the preformed fibril model. In this model, fibrils prepared from recombinant αsyn induce misfolding of
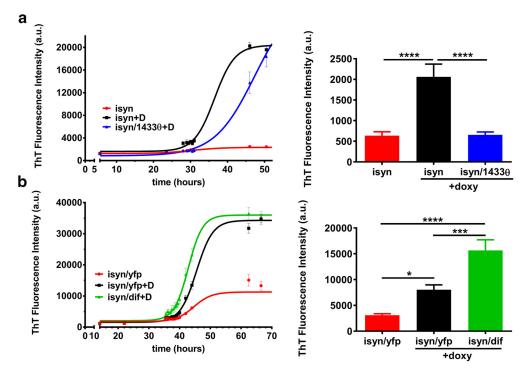
Figure 9. 14-3-3θ reduces seeding potential of released αsyn. ***a***, Effect of 14-3-3θ overexpression on seeding potential of αsyn-enriched CM. αSyn fibril formation was measured by the enhancement over time of ThT fluorescence intensity. Left hand graph shows time lapse curves of ThT fluorescence intensity measurements during PMCA assay of recombinant αsyn treated with CM from isyn or isyn/14-3-3θ cells. Right hand graph shows ThT fluorescence intensity at 31 h. $n = 3$ rounds with eight replicates per round. ****$p < 0.0001$ (Tukey's multiple-comparison test). ***b***, Effect of 14-3-3 inhibition on seeding potential of αsyn-enriched CM. Left hand graph shows time lapse curves of ThT fluorescence intensity measurements during PMCA assay of recombinant αsyn treated with CM from isyn/difopein-eYFP (isyn/dif) and isyn/mutant difopein-eYFP (isyn/yfp) control cells. Right graph shows ThT fluorescence intensity at 42 h. $n = 3$ rounds with eight replicates per round. *$p = 0.027$, ***$p = 0.0003$, ****$p < 0.0001$ (Tukey's multiple-comparison test).
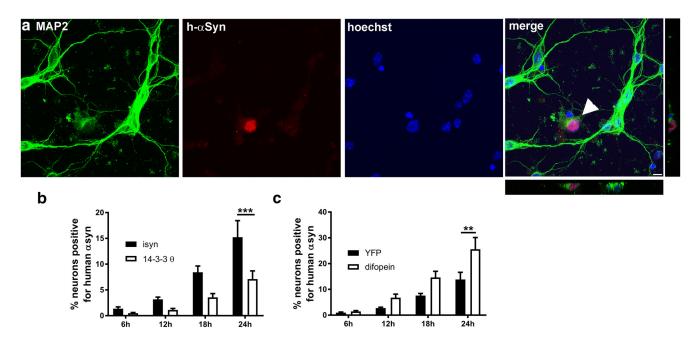

Figure 10. 14-3-3θ blocks uptake and internalization of released αsyn by primary neurons. ***a***, Confocal microscopy demonstrating immunocytochemistry for human αsyn (red) and MAP2 (green) in primary hippocampal neurons treated with CM from induced isyn/difopein-eYFP at 24 h after treatment. Arrow shows dying neuron that has internalized human αsyn. Scale bar, 10 μm. ***b***, Quantification of percentage of primary neurons that are positive for human αsyn immunoreactivity after treatment with CM from induced isyn or isyn/14-3-3θ cells. $n = 3$ independent rounds with 2 replicates per round. ***$p = 0.0007$ (Tukey's multiple-comparison test). ***c***, Quantification of percentage of primary neurons that are positive for human αsyn immunoreactivity after treatment with CM from induced isyn/difopein-eYFP or isyn/mutant difopein-eYFP control cells. $n = 3$ independent rounds with two replicates per round. **$p = 0.0016$ (Tukey's multiple-comparison test). Error bars represent SEM.
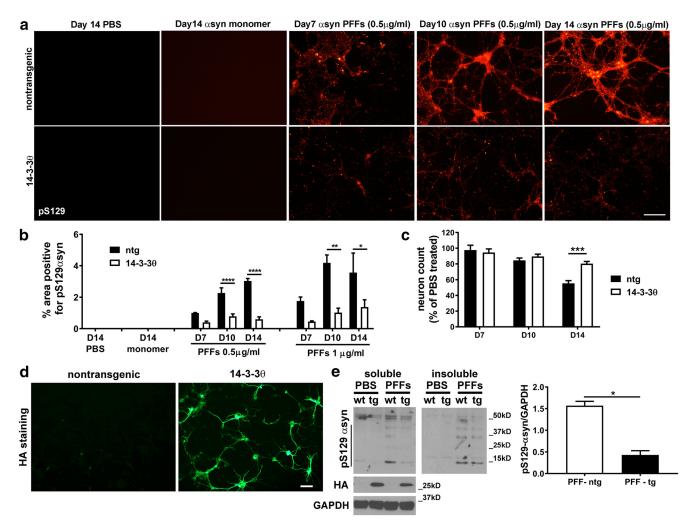
Figure 11. 14-3-3θ reduces whereas 14-3-3 inhibition promotes formation of pathologic, insoluble αsyn aggregates by PFF treatment. **a**, Immunocytochemistry for pS129-αsyn in primary hippocampal cultures from nontransgenic and 14-3-3θ transgenic mouse littermates. Neurons were treated with PBS, monomeric αsyn, or PFFs at 5 DIV and then fixed with Triton X-100 in the fixative to stain for insoluble, pS129-positive αsyn. Scale bar, 100 μm. **b**, Quantification of area covered by pS129-αsyn immunoreactivity in primary cultures from nontransgenic and 14-3-3θ transgenic mice treated with PBS, monomeric αsyn, or PFFs. n = 3 independent rounds with two replicates per round. *p = 0.045, **p = 0.0025, ****p < 0.0001 (Sidak's multiple-comparison test). **c**, Neuronal counts of primary neurons from nontransgenic and 14-3-3θ mice treated with 1 μg/ml PFFs. n = 3 independent rounds with two replicates per round. ***p = 0.0004 (Sidak's multiple-comparison test). **d**, Immunocytochemistry for the HA epitope in primary hippocampal neurons from nontransgenic and HA-tagged 14-3-3θ transgenic mouse pups. Scale bar, 100 μm. **e**, Western blot for pS129 αsyn in Triton X-100 soluble and insoluble cell lysates prepared from primary neurons treated with PBS or PFFs for 14 d. Wt, Wild-type; tg, 14-3-3θ. Longitudinal bar next to pS129 αsyn blot shows soluble pS129 αsyn bands quantified. n = 2 independent rounds. *p = 0.0148 (Student's t test). Error bars represent SEM.

endogenous αsyn that results in Lewy body/Lewy neurite-like pathology in primary neurons (Volpicelli-Daley et al., 2011, 2014). Aggregation of αsyn is associated with insolubilization and phosphorylation of endogenous αsyn at S129, and fibrils cannot induce these changes in neurons from αsyn knock-out mice, pointing to misfolding of endogenous αsyn (Volpicelli-Daley et al., 2011). We first tested the ability of human αsyn PFFs to induce pathologic aggregation in primary hippocampal cultures from nontransgenic and 14-3-3θ transgenic mice, which demonstrated HA-tagged 14-3-3θ expression in the hippocampus (Fig. 11d; Lavalley et al., 2016). Treatment of nontransgenic cultures with PFFs induced the formation of Triton X-100 insoluble inclusions that were positive for S129-phosphorylated (pS129) αsyn, and the amount of pS129-αsyn-positive aggregation increased over time, as previously described (Fig. 11a,b). Neither PBS nor monomeric αsyn induced any pS129-αsyn signal (Fig. 11a,b). The amount of pS129-αsyn staining was dramatically reduced in 14-3-3θ transgenic neurons treated with 0.5 μg/ml PFFs at 10 and 14 d after PFF treatment (Fig. 11a,b; two-

way ANOVA, genotype: $F_{(1,29)} = 102$, $p < 0.0001$; time: $F_{(2,29)} = 19.51$, $p < 0.0001$; interaction: $F_{(2,29)} = 12.53$, $p = 0.0001$). Similar results were observed with 1 μg/ml PFF treatment at 10 and 14 d (Fig. 11b; two-way ANOVA, genotype: $F_{(1,30)} = 20.45$, $p < 0.0001$; time: $F_{(2,30)} = 3.789$, $p = 0.0341$; interaction: $F_{(2,30)} = 1.177$, $p = 0.3219$). Western blot analysis confirmed these findings, with less pS129 αsyn in the soluble and insoluble fractions from 14-3-3θ neurons compared with nontransgenic neurons treated with PFFs (Fig. 11e; unpaired, two-tailed t test: $t_{(2)} = 8.14$, $p = 0.0148$).

PFF treatment induces significant neuronal death at 14 d after PFF treatment, after the initiation of αsyn aggregation (Volpicelli-Daley et al., 2011). We measured neuronal counts in primary neuronal cultures treated with PFFs at 1 μg/ml, and observed a 45% loss in neuronal counts in nontransgenic cultures treated with PFFs compared with those treated with PBS (Fig. 11c). Neuronal loss induced by PFFs was mitigated to 20% in 14-3-3θ neuronal cultures (Fig. 11c; two-way ANOVA, genotype:
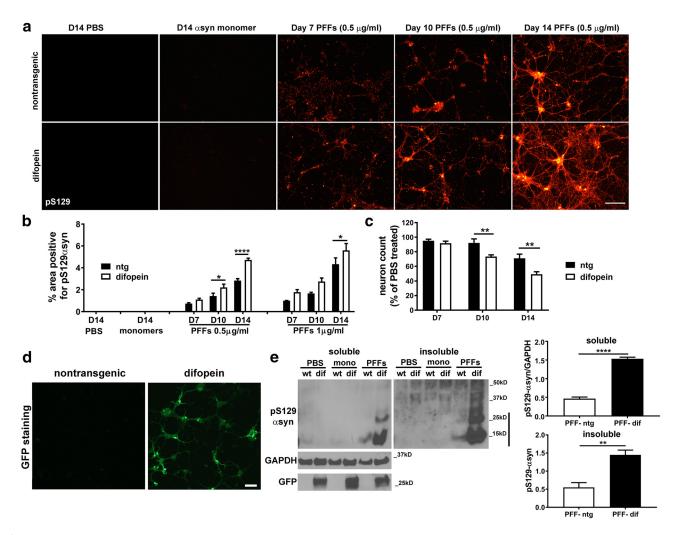
Figure 12. 14-3-3 inhibition promotes formation of pathologic, insoluble αsyn aggregates by PFF treatment. ***a***, Immunocytochemistry for pS129-αsyn in primary hippocampal cultures from nontransgenic and difopein-eYFP transgenic mouse littermates. Neurons were treated with PBS, monomeric αsyn, or PFFs at 5 DIV and then fixed with Triton X-100 in the fixative to stain for insoluble, pS129-positive αsyn. Scale bar, 100 μm. ***b***, Quantification of area covered by pS129-αsyn immunoreactivity in primary cultures from nontransgenic and difopein-eYFP transgenic mice treated with PBS, monomeric αsyn, or PFFs. $n = 4$ independent rounds with two replicates per round. *$p < 0.05$, ****$p < 0.0001$ (Sidak's multiple-comparison test). Error bars represent SEM. ***c***, Neuronal counts of primary neurons from nontransgenic and difopein-eYFP mice treated with 0.5 μg/ml PFFs. $n = 3$ independent rounds with two replicates per round. **$p < 0.01$ (Sidak's multiple-comparison test). Error bars represent SEM. ***d***, Immunocytochemistry for GFP in primary hippocampal neurons from nontransgenic and difopein-eYFP transgenic mouse pups. Scale bar, 100 μm. ***e***, Western blot for pS129 and total αsyn in Triton X-100 soluble and insoluble cell lysates prepared from primary neurons treated with PBS, αsyn monomer, or PFFs for 14 d. Wt, Wild-type; dif, difopein. Longitudinal bar next to pS129 αsyn blot shows pS129 αsyn bands quantified. Arrows point out pS129 αsyn bands. $n = 3$ independent rounds. **$p = 0.0085$, ****$p < 0.0001$ (Student's t test). Error bars represent SEM.

$F_{(1,30)} = 7.431$, $p = 0.0106$; time: $F_{(2,30)} = 25.86$, $p < 0.0001$; interaction: $F_{(2,30)} = 6.456$, $p = 0.0047$).

We next examined the effect of 14-3-3 inhibition on PFF-induced aggregation and neuronal death. Hippocampal cultures from difopein-eYFP transgenic mice, which have difopein-eYFP expression in the hippocampus (Fig. 12*d*; Lavalley et al., 2016), showed no evidence of pS129-αsyn staining in response to PBS or monomeric αsyn staining (Fig. 12*a*,*b*). pS129-αsyn-positive aggregation was increased in difopein neurons treated with 0.5 μg/ml PFFs compared with nontransgenic neurons (Fig. 12*a*,*b*; two-way ANOVA, genotype: $F_{(1,30)} = 40.17$, $p < 0.0001$; time: $F_{(2,30)} = 111.8$, $p < 0.0001$; interaction: $F_{(2,30)} = 7.966$, $p = 0.0017$). pS129-αsyn-positive aggregation was also increased in difopein neurons treated with 1 μg/ml PFFs (Fig. 12*b*; two-way ANOVA, genotype: $F_{(1,42)} = 10.63$, $p = 0.0022$; time: $F_{(2,42)} = 48.28$, $p < 0.0001$; interaction: $F_{(2,42)} = 0.5827$, $p = 0.5628$) but not as dramatically, potentially suggesting a upper limit to the amount of aggregation that can be induced. Western blot analysis showed an increase in pS129-αsyn levels in the lysates from difo-

pein neurons treated with PFFs compared with nontransgenic neurons (Fig. 12*e*; soluble fraction: unpaired, two-tailed t test: $t_{(4)} = 18.19$, $p < 0.0001$; insoluble fraction: unpaired, two-tailed t test: $t_{(4)} = 4.82$, $p = 0.0085$). Neuronal loss induced by PFFs was observed earlier in difopein cultures at 10 d after PFF treatment at 0.5 μg/ml, at a time point when neuronal loss is normally not observed in wild-type cultures (Fig. 12*c*; two-way ANOVA, genotype: $F_{(1,30)} = 21.37$, $p < 0.0001$; time: $F_{(2,30)} = 38.37$, $p < 0.0001$; interaction: $F_{(2,30)} = 3.256$, $p = 0.0525$). At 14 d after treatment, difopein cultures showed a 31% increase in neuronal death compared with nontransgenic cultures (Fig. 12*c*).

14-3-3θ reduces propagation in the preformed fibril model

To test whether 14-3-3θ can block cell-to-cell spread of pathogenic αsyn in the PFF model, we used microfluidic culture devices with three separate compartments connected by microgrooves. We plated nontransgenic or 14-3-3θ neurons in the first compartment and nontransgenic neurons into the second and third compartments (Fig. 13*b*). PFFs were added to the first com-
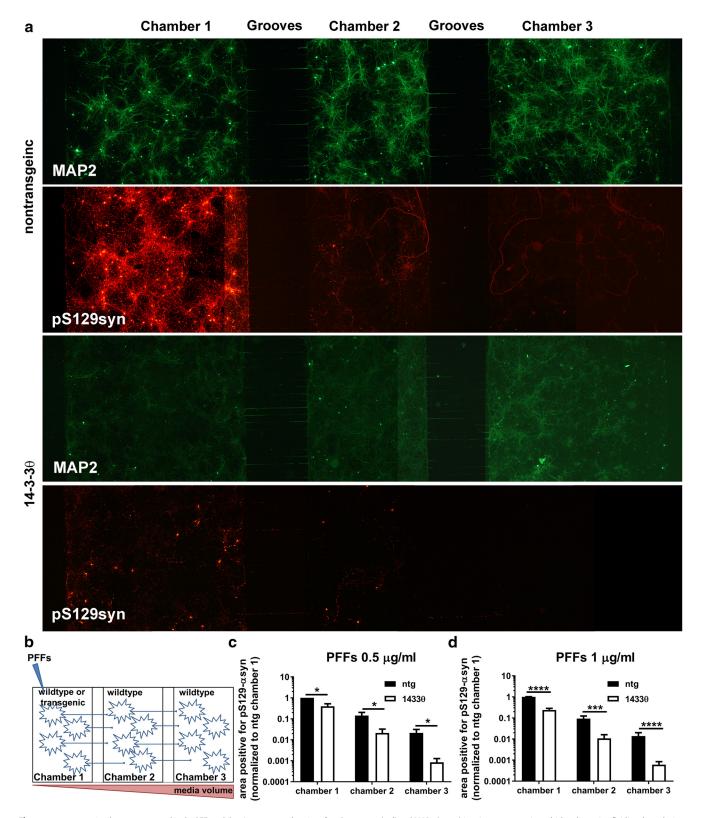
Figure 13. 14-3-3θ reduces αsyn spread in the PFF model. ***a***, Immunocytochemistry for pS129-αsyn (red) and MAP2 (green) in primary neurons in multichamber, microfluidic culture devices. Primary neurons from nontransgenic or 14-3-3θ mice were plated in chamber 1, and nontransgenic mouse neurons were plated in the other chambers of multichamber, microfluidic devices. Neurons in chamber 1 were treated with 0.5 μg/ml PFFs. ***b***, Schematic of experimental design. Neurons from nontransgenic or 14-3-3θ mice were plated in chamber 1, and nontransgenic mouse neurons were plated in chambers 2 and 3. At DIV5, neurons in chamber 1 were treated with PFFs. Spread of PFFs into the other chambers was prevented by hydrostatic pressure differences between chambers. ***c***, Quantification of area covered by pS129-αsyn immunoreactivity in each chamber of primary cultures from nontransgenic and 14-3-3θ transgenic mice treated with 0.5 μg/ml PFFs. $n = 4$. ***d***, Quantification of area covered by pS129-αsyn immunoreactivity in each chamber of primary cultures from nontransgenic and 14-3-3θ transgenic mice treated with 1 μg/ml PFFs. $n = 8$. *$p < 0.05$, ***$p < 0.001$, ****$p < 0.0001$ (Student's t-test, with correction for multiple comparisons using Holm-Sidak method; adjusted p values shown). Error bars represent SEM.
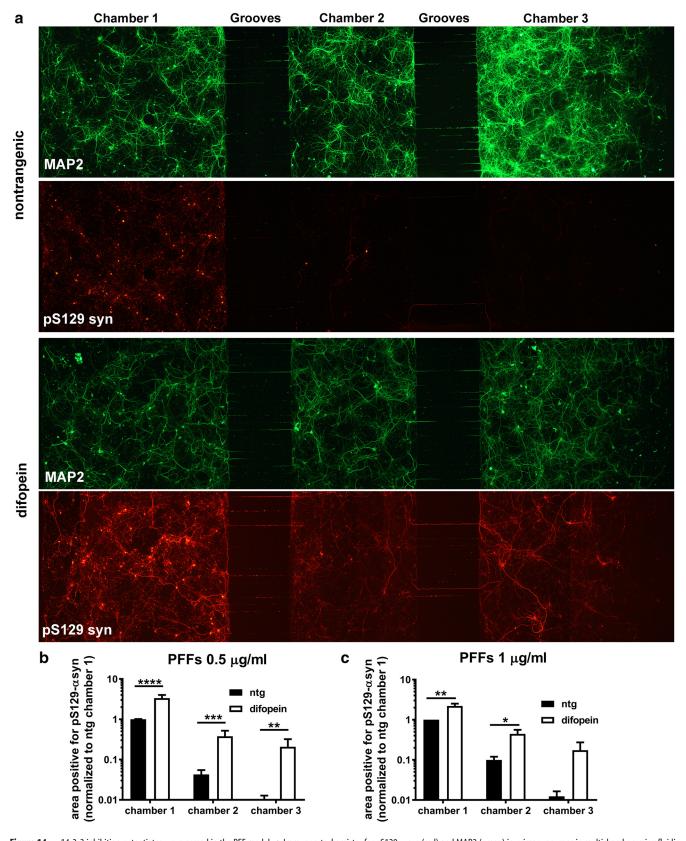
Figure 14. 14-3-3 inhibition potentiates αsyn spread in the PFF model. ***a***, Immunocytochemistry for pS129-αsyn (red) and MAP2 (green) in primary neurons in multichamber, microfluidic culture devices. Primary neurons from nontransgenic or difopein mice were plated in Chamber 1, and nontransgenic mouse neurons were plated in Chambers 2 and 3. At 5 DIV, neurons in Chamber 1 were treated with 1 μg/ml PFFs. Staining in chamber plated with wild-type neurons appears less intense than in Figure 13 because the images here were captured at a lower exposure to prevent saturation of the pS129-αsyn signal in the difopein chamber. ***b***, Quantification of area covered by pS129-αsyn immunoreactivity in each chamber of primary cultures from nontransgenic and difopein transgenic mice treated with 0.5 μg/ml PFFs. $n = 7$. ***c***, Quantification of area covered by pS129-αsyn immunoreactivity in each chamber of primary cultures from nontransgenic and difopein transgenic mice treated with 1 μg/ml PFFs. $n = 4$. *$p < 0.05$, **$p < 0.01$, ***$p < 0.001$, ****$p < 0.0001$ (Student's t test with correction for multiple comparisons using Holm–Sidak method; adjusted p values shown). Error bars represent SEM.
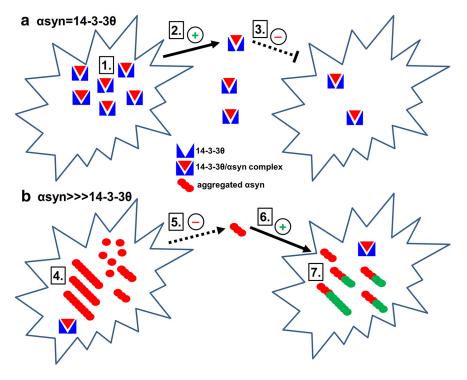
a αsyn=14-3-3θ

b αsyn>>>14-3-3θ

Figure 15. Model for 14-3-3θ's effects on αsyn propagation. **a**, Under normal circumstances, 14-3-3θ prevents intracellular αsyn aggregation by acting as a chaperone to prevent misfolding of intracellular αsyn (1) and by promoting the release of αsyn (2). Extracellularly, αsyn is complexed with 14-3-3θ which prevents its uptake and seeding in surrounding neurons (3). **b**, In the disease state, there is a deficiency of 14-3-3θ compared with αsyn. 14-3-3θ no longer adequately acts as a chaperone to prevent αsyn misfolding (4). In addition, with reduced levels of 14-3-3θ, less αsyn is released such that more misfolding αsyn substrate remains intracellularly to initiate more misfolding (5). Any αsyn that is released is not adequately complexed with 14-3-3θ and is available for uptake by surrounding neurons (6). αSyn that is taken up by surrounding neurons has seeding capabilities and induces the misfolding of αsyn (green) in these neurons (7).

partment at DIV5 (Fig. 13b). PFF spread into the other compartments is prevented by hydrostatic pressure differences between compartments (Park et al., 2006). At 14 d after PFF treatments, pS129-αsyn was detectable in all three chambers when nontransgenic neurons were plated in all three compartments, with a gradient of highest pS129-αsyn in Chamber 1 to lowest pS129-αsyn in the most distal chamber (Fig. 13a,c,d). When 14-3-3θ neurons were plated in the first compartment and treated with 0.5 μg/ml PFFs, pS129-αsyn staining was dramatically reduced in all three compartments, with almost no detectable pS129-αsyn in Chambers 2 and 3 (Fig. 13c; unpaired, two-tailed t test corrected for multiple comparisons by Holm–Sidak method; Chamber 1: $t_{(6)} = 3.547$, adjusted $p = 0.0359$; Chamber 2: $t_{(6)} = 2.679$, adjusted $p = 0.0366$; Chamber 3: $t_{(5)} = 3.769$, $p = 0.0359$). Similar results were observed when neurons were treated with 1 μg/ml PFFs (Fig. 13a,d; unpaired, two-tailed t test corrected for multiple comparisons by Holm–Sidak method; Chamber 1: $t_{(14)} = 8.001$, adjusted $p < 0.0001$; Chamber 2: $t_{(14)} = 5.033$, adjusted $p = 0.00018$; Chamber 3: $t_{(14)} = 7.126$, $p < 0.0001$). Conversely, when difopein neurons were plated in the first compartment, we saw a significant increase in pS129-αsyn-positive aggregates in Chambers 2 and 3 compared with microfluidic devices plated with only nontransgenic neurons in all chambers at 14 d after 0.5 μg/ml PFF treatment (Fig. 14b; unpaired, two-tailed t test corrected for multiple comparisons by Holm–Sidak method; Chamber 1: $t_{(12)} = 6.879$, adjusted $p < 0.0001$; Chamber 2: $t_{(12)} = 4.797$, adjusted $p = 0.00087$; Chamber 3: $t_{(12)} = 4.209$, $p = 0.00121$) or 1 μg/ml PFF treatment (Fig. 14a,c; unpaired, two-tailed t test corrected for multiple comparisons by Holm–Sidak method;

Chamber 1: $t_{(6)} = 5.369$, adjusted $p = 0.00513$; Chamber 2: $t_{(6)} = 3.879$, adjusted $p = 0.0163$; Chamber 3: $t_{(6)} = 1.935$, $p = 0.101$).

Discussion

Our data demonstrates that 14-3-3θ regulates the pathologic transmission and toxicity of αsyn in two different αsyn models. Using a paracrine model, we observed that 14-3-3θ overexpression in isyn cells blocked αsyn oligomerization, seeding, and toxicity, whereas 14-3-3 inhibition in isyn cells promoted αsyn oligomerization, seeding, and toxicity. In the fibril model, αsyn fibrils induced less αsyn aggregation and neuron loss in 14-3-3θ cultures, whereas 14-3-3 inhibition accelerated αsyn aggregation and neuron death. The ability of 14-3-3θ to reduce αsyn spread from neuron to neuron was highlighted by our studies in multichamber devices. 14-3-3 inhibition promoted spread of αsyn pathology to distal chamber neurons not exposed directly to αsyn fibrils, whereas 14-3-3θ overexpression blocked the spread to distal chamber neurons.

The advantage of the paracrine model is that it allows us to tease apart the different cellular processes required for spread, including release, seeding, and uptake. Our studies in the paracrine model illustrate the mechanisms by which 14-3-3θ regulates pathogenic αsyn spread. Our findings point to 14-3-3θ as a chaperone to regulate αsyn propagation: despite promoting αsyn release, 14-3-3θ was complexed with released αsyn and the released αsyn was less likely to oligomerize or promote αsyn seeding. This conformational change in αsyn by the presence of 14-3-3θ also prevented αsyn internalization and/or promoted αsyn degradation by surrounding neurons.

These findings point to the following model of 14-3-3θ as an endogenous regulator of pathogenic αsyn transmission (Fig. 15). Under normal conditions, we propose 14-3-3θ levels are sufficient to promote normal αsyn folding and prevent its ability to take on conformations that promote seeding. Misfolded αsyn molecule is secreted by 14-3-3θ-dependent mechanisms to prevent its interaction with normally folded intracellular αsyn molecules and thus reduce the likelihood of intracellular propagation. Any released αsyn is complexed with 14-3-3θ which can help to refold αsyn into a less seed-competent state. As a result, 14-3-3θ may reduce the uptake of released αsyn by other neurons and/or indirectly promotes its degradation if internalized. 14-3-3θ could potentially interfere with αsyn uptake through cell surface receptors, such as LAG3 (Mao et al., 2016).

Under conditions in which αsyn levels are increased, the amount of 14-3-3θ is not sufficient to appropriately regulate αsyn folding. Indeed the stoichiometric ratio of αsyn to 14-3-3s is critical in 14-3-3s' ability to regulate αsyn *in vitro* (Plotegher et al., 2014). With a reduction in 14-3-3θ, less αsyn is released extracellularly, thus potentially allowing for more intracellular misfolded αsyn substrate molecules to potentiate intracellular misfolding. Although αsyn release may be reduced under low

14-3-3θ conditions, any αsyn that is released is not appropriately complexed with 14-3-3θ and takes on a pathologic conformation that promotes its oligomerization, seeding, and uptake as supported our data. Overexpression of 14-3-3θ is able to reestablish this homeostatic process: when we overexpress 14-3-3θ in the presence of excess αsyn, 14-3-3θ resets the cellular balance by refolding intracellular αsyn directly through chaperone function and potentially indirectly by kicking out aggregation-prone αsyn out of the cell. Any released αsyn is complexed with 14-3-3θ to reduce its seeding potential and uptake.

Whether low 14-3-3 levels are a prerequisite to initiate αsyn transmission or if they perpetuate αsyn propagation after the process has first started is unknown. An age-related reduction in soluble 14-3-3 levels has been observed in *Caenorhabditis elegans* and rodent aging models (David et al., 2010; VanGuilder et al., 2011). Low 14-3-3s during aging could set the stage for αsyn misfolding, which could be accelerated by other genetic and environmental factors. Another possibility is that other processes, such as age-related dysfunction of protein degradation (Tonoki et al., 2009; Yamaguchi and Otsu, 2012; Tan et al., 2014), lead to elevated αsyn levels which then causes the reduction in 14-3-3 levels; leading to a vicious cycle to further potentiate αsyn pathology. We previously showed that elevated αsyn reduces 14-3-3 expression in cellular and mouse αsyn models (Yacoubian et al., 2010; Ding et al., 2013). We also observed reduced soluble 14-3-3 levels in human DLB (McFerrin et al., 2017), yet whether this occurs early or late in the disease process is unknown. Whether misfolded αsyn or low 14-3-3 levels initiate the process, it is clear that the balance of 14-3-3θ levels to αsyn levels is critical to slowing or accelerating αsyn propagation.

A surprising finding is that an increase in the total amount of αsyn released into the CM did not translate to increased toxicity as one may predict. Our studies reveal that αsyn release is required for non-cell autonomous αsyn toxicity but is not sufficient. The form of αsyn released is critical; based on our data, release of oligomeric and seed-competent αsyn is implicated in toxicity. Buffering of released αsyn with chaperones such as 14-3-3s may allow for the release of misfolded αsyn from cells in which it is produced without causing inadvertent "friendly fire" toxicity to normal neighboring neurons. In the disease state, levels of 14-3-3s are relatively reduced compared with excess αsyn and thus could fail to buffer misfolded αsyn. 14-3-3θ overexpression reduces oligomerization and seeding capability of released αsyn in our studies.

Our findings suggesting that 14-3-3θ reduces αsyn internalization also point to the likelihood that uptake of αsyn is also important to its toxicity. We hypothesize that uptake of released αsyn in the paracrine model causes seeding of endogenous αsyn into aggregates and ultimately toxicity, similar to that observed in the fibril model. However, we cannot rule out the possibility that released αsyn could cause direct neuronal death that is not dependent on uptake into the cytoplasm. Additionally, our data showing a reduction in staining for human αsyn in neurons exposed to CM from 14-3-3θ-overexpressing isyn cells (Fig. 10) may instead reflect alterations in protein degradation instead of differences in uptake. Human αsyn in the CM from isyn cells overexpressing 14-3-3θ may be more readily degraded in exposed neurons, possibly due to its conformation state.

αSyn associated with exosomes was not toxic in our paracrine model, in contrast to other studies suggesting that αsyn release through exosomes is responsible for αsyn toxicity (Emmanouilidou et al., 2010; Danzer et al., 2012; Stuendl et al., 2016; Ngolab et al., 2017). Only ~0.6% of total αsyn was found in the exosomes

when released from isyn cells. It is unclear whether αsyn released by the non-exosomal fraction has properties that make it more toxic, or whether it is the relative quantity of pathogenic αsyn released that is responsible for the difference noted in the toxicities of these fractions. Multiple release mechanisms, including possibly exosomal release, are likely responsible for αsyn release and could vary between different neuronal populations and at different stages of disease.

In conclusion, 14-3-3θ regulates αsyn transmission in two separate αsyn models. Given evidence that 14-3-3s are reduced in αsyn models and disease, methods to restore 14-3-3 function could serve as a means to reduce αsyn propagation in synucleinopathies.

References

Abdelmotilib H, Maltbie T, Delic V, Liu Z, Hu X, Fraser KB, Moehle MS, Stoyka L, Anabtawi N, Krendelchtchikova V, Volpicelli-Daley LA, West A (2017) α-Synuclein fibril-induced inclusion spread in rats and mice correlates with dopaminergic neurodegeneration. Neurobiol Dis 105:84–98. CrossRef Medline

Abounit S, Bousset L, Loria F, Zhu S, de Chaumont F, Pieri L, Olivo-Marin JC, Melki R, Zurzolo C (2016) Tunneling nanotubes spread fibrillar alpha-synuclein by intercellular trafficking of lysosomes. EMBO J 35:2120–2138. CrossRef Medline

Alvarez-Erviti L, Seow Y, Schapira AH, Gardiner C, Sargent IL, Wood MJ, Cooper JM (2011) Lysosomal dysfunction increases exosome-mediated alpha-synuclein release and transmission. Neurobiol Dis 42:360–367. CrossRef Medline

Becker K, Wang X, Vander Stel K, Chu Y, Kordower J, Ma J (2018) Detecting Alpha Synuclein Seeding Activity in Formaldehyde-Fixed MSA Patient Tissue by PMCA. Mol Neurobiol. Advance online publication. Retrieved Mar 12, 2018. doi: 10.1007/s12035–018-1007-y.

Berg D, Riess O, Bornemann A (2003) Specification of 14-3-3 proteins in Lewy bodies. Ann Neurol 54:135. CrossRef Medline

Chutna O, Goncalves S, Villar-Piqué A, Guerreiro P, Marijanovic Z, Mendes T, Ramalho J, Emmanouilidou E, Ventura S, Klucken J, Barral DC, Giorgini F, Vekrellis K, Outeiro TF (2014) The small GTPase Rab11 co-localizes with alpha-synuclein in intracellular inclusions and modulates its aggregation, secretion and toxicity. Hum Mol Genet 23:6732–6745. CrossRef Medline

Danzer KM, Ruf WP, Putcha P, Joyner D, Hashimoto T, Glabe C, Hyman BT, McLean PJ (2011) Heat-shock protein 70 modulates toxic extracellular alpha-synuclein oligomers and rescues trans-synaptic toxicity. FASEB J 25:326–336. CrossRef Medline

Danzer KM, Kranich LR, Ruf WP, Cagsal-Getkin O, Winslow AR, Zhu L, Vanderburg CR, McLean PJ (2012) Exosomal cell-to-cell transmission of alpha synuclein oligomers. Mol Neurodegener 7:42. CrossRef Medline

David DC, Ollikainen N, Trinidad JC, Cary MP, Burlingame AL, Kenyon C (2010) Widespread protein aggregation as an inherent part of aging in *C. elegans*. PLoS Biol 8: e1000450. CrossRef Medline

Dearborn AD, Wall EA, Kizziah JL, Klenow L, Parker LK, Manning KA, Spilman MS, Spear JM, Christie GE, Dokland T (2017) Competing scaffolding proteins determine capsid size during mobilization of staphylococcus aureus pathogenicity islands. eLife 6:e30822. CrossRef Medline

Desplats P, Lee HJ, Bae EJ, Patrick C, Rockenstein E, Crews L, Spencer B, Masliah E, Lee SJ (2009) Inclusion formation and neuronal cell death through neuron-to-neuron transmission of alpha-synuclein. Proc Natl Acad Sci U S A 106:13010–13015. CrossRef Medline

Ding H, Fineberg NS, Gray M, Yacoubian TA (2013) α-Synuclein overexpression represses 14-3-3θ transcription. J Mol Neurosci 51:1000–1009. CrossRef Medline

Ding H, Underwood R, Lavalley N, Yacoubian TA (2015) 14-3-3 inhibition promotes dopaminergic neuron loss and 14-3-3θ overexpression promotes recovery in the MPTP mouse model of Parkinson's disease. Neuroscience 307:73–82. CrossRef Medline

Dzamko N, Deak M, Hentati F, Reith AD, Prescott AR, Alessi DR, Nichols RJ (2010) Inhibition of LRRK2 kinase activity leads to dephosphorylation of Ser(910)/Ser(935), disruption of 14-3-3 binding and altered cytoplasmic localization. Biochem J 430:405– 413. CrossRef Medline

Emmanouilidou E, Melachroinou K, Roumeliotis T, Garbis SD, Ntzouni M,

Margaritis LH, Stefanis L, Vekrellis K (2010) Cell-produced alpha-synuclein is secreted in a calcium-dependent manner by exosomes and impacts neuronal survival. J Neurosci 30:6838–6851. CrossRef Medline

Fauvet B, Mbefo MK, Fares MB, Desobry C, Michael S, Ardah MT, Tsika E, Coune P, Prudent M, Lion N, Eliezer D, Moore DJ, Schneider B, Aebischer P, El-Agnaf OM, Masliah E, Lashuel H (2012) α-Synuclein in central nervous system and from erythrocytes, mammalian cells, and *Escherichia coli* exists predominantly as disordered monomer. J Biol Chem 287:15345–15364. CrossRef Medline

Foote M, Qiao H, Graham K, Wu Y, Zhou Y (2015) Inhibition of 14-3-3 proteins leads to schizophrenia-related behavioral phenotypes and synaptic defects in mice. Biological psychiatry 78:386–395. CrossRef Medline

Fraser KB, Moehle MS, Daher JP, Webber PJ, Williams JY, Stewart CA, Yacoubian TA, Cowell RM, Dokland T, Ye T, Chen D, Siegal GP, Galemmo RA, Tsika E, Moore DJ, Standaert DG, Kojima K, Mobley JA, West AB (2013) LRRK2 secretion in exosomes is regulated by 14-3-3. Hum Mol Genet 22:4988–5000. CrossRef Medline

Gonçalves SA, Macedo D, Raquel H, Simões PD, Giorgini F, Ramalho JS, Barral DC, Ferreira Moita L, Outeiro TF (2016) shRNA-based screen identifies endocytic recycling pathway components that act as genetic modifiers of α-synuclein aggregation, secretion and toxicity. PLoS genetics 12, e1005995. CrossRef Medline

Hansen C, Angot E, Bergström AL, Steiner JA, Pieri L, Paul G, Outeiro TF, Melki R, Kallunki P, Fog K, Li JY, Brundin P (2011) alpha-synuclein propagates from mouse brain to grafted dopaminergic neurons and seeds aggregation in cultured human cells. J Clin Invest 121:715–725. CrossRef Medline

Hasegawa T, Konno M, Baba T, Sugeno N, Kikuchi A, Kobayashi M, Miura E, Tanaka N, Tamai K, Furukawa K, Arai H, Mori F, Wakabayashi K, Aoki M, Itoyama Y, Takeda A (2011) The AAA-ATPase VPS4 regulates extracellular secretion and lysosomal targeting of alpha-synuclein. PLoS One 6:e29460. CrossRef Medline

Herva ME, Zibaee S, Fraser G, Barker RA, Goedert M, Spillantini MG (2014) Anti-amyloid compounds inhibit alpha-synuclein aggregation induced by protein misfolding cyclic amplification (PMCA). J Biol Chem 289: 11897–11905. CrossRef Medline

Jang A, Lee HJ, Suk JE, Jung JW, Kim KP, Lee SJ (2010) Non-classical exocytosis of alpha-synuclein is sensitive to folding states and promoted under stress conditions. J Neurochem 113:1263–1274. CrossRef Medline

Kajiwara Y, Buxbaum JD, Grice DE (2009) SLITRK1 binds 14-3-3 and regulates neurite outgrowth in a phosphorylation-dependent manner. Biol Psychiatry 66:918–925. CrossRef Medline

Kaplan A, Morquette B, Kroner A, Leong S, Madwar C, Sanz R, Banerjee SL, Antel J, Bisson N, David S, Fournier AE (2017) Small-molecule stabilization of 14-3-3 protein-protein interactions stimulates axon regeneration. Neuron 93:1082–1093.e5. CrossRef Medline

Kawamoto Y, Akiguchi I, Nakamura S, Honjyo Y, Shibasaki H, Budka H (2002) 14-3-3 proteins in Lewy bodies in Parkinson disease and diffuse Lewy body disease brains. J Neuropathol Exp Neurol 61:245–253. CrossRef Medline

Kordower JH, Chu Y, Hauser RA, Freeman TB, Olanow CW (2008) Lewy body-like pathology in long-term embryonic nigral transplants in Parkinson's disease. Nat Med 14:504–506. CrossRef Medline

Lashuel HA, Overk CR, Oueslati A, Masliah E (2013) The many faces of alpha-synuclein: from structure and toxicity to therapeutic target. Nat Rev Neurosci 14:38–48. CrossRef Medline

Lavalley NJ, Slone SR, Ding H, West AB, Yacoubian TA (2016) 14-3-3 proteins regulate mutant LRRK2 kinase activity and neurite shortening. Hum Mol Genet 25:109–122. CrossRef Medline

Lee HJ, Patel S, Lee SJ (2005) Intravesicular localization and exocytosis of α-synuclein and its aggregates. J Neurosci 25:6016–6024. CrossRef Medline

Lee HJ, Cho ED, Lee KW, Kim JH, Cho SG, Lee SJ (2013) Autophagic failure promotes the exocytosis and intercellular transfer of alpha-synuclein. Exp Mol Med 45:e22. CrossRef Medline

Li X, Wang QJ, Pan N, Lee S, Zhao Y, Chait BT, Yue Z (2011) Phosphorylation-dependent 14-3-3 binding to LRRK2 is impaired by common mutations of familial Parkinson's disease. PLoS One 6:e17153. CrossRef Medline

Liu J, Zhang JP, Shi M, Quinn T, Bradner J, Beyer R, Chen S, Zhang J (2009) Rab11a and HSP90 regulate recycling of extracellular alpha-synuclein. J Neurosci 29:1480–1485. CrossRef Medline

Luk KC, Kehm V, Carroll J, Zhang B, O'Brien P, Trojanowski JQ, Lee VM (2012) Pathological α-synuclein transmission initiates Parkinson-like neurodegeneration in nontransgenic mice. Science 338:949–953. CrossRef Medline

Mao X, Ou MT, Karuppagounder SS, Kam TI, Yin X, Xiong Y, Ge P, Umanah GE, Brahmachari S, Shin JH, Kang HC, Zhang J, Xu J, Chen R, Park H, Andrabi SA, Kang SU, Gonçalves RA, Liang Y, Zhang S, et al. (2016) Pathological α-synuclein transmission initiated by binding lymphocyte-activation gene 3. Science 353:aah3374. CrossRef Medline

Marzinke MA, Mavencamp T, Duratinsky J, Clagett-Dame M (2013) 14-3-3epsilon and NAV2 interact to regulate neurite outgrowth and axon elongation. Arch Biochem Biophys 540:94–100. CrossRef Medline

Masters SC, Fu H (2001) 14-3-3 proteins mediate an essential anti-apoptotic signal. J Biol Chem 276:45193–45200. CrossRef Medline

Masuda-Suzukake M, Nonaka T, Hosokawa M, Kubo M, Shimozawa A, Akiyama H, Hasegawa M (2014) Pathological α-synuclein propagates through neural networks. Acta Neuropathol Commun 2:88. CrossRef Medline

McFerrin MB, Chi X, Cutter G, Yacoubian TA (2017) Dysregulation of 14-3-3 proteins in neurodegenerative diseases with Lewy body or Alzheimer pathology. Ann Clin Transl Neurol 4:466–477. CrossRef Medline

Mrowiec T, Schwappach B (2006) 14-3-3 proteins in membrane protein transport. Biol Chem 387:1227–1236. CrossRef Medline

Ngolab J, Trinh I, Rockenstein E, Mante M, Florio J, Trejo M, Masliah D, Adame A, Masliah E, Rissman RA (2017) Brain-derived exosomes from dementia with Lewy bodies propagate alpha-synuclein pathology. Acta Neuropathol Commun 5:46. CrossRef Medline

Nichols RJ, Dzamko N, Morrice NA, Campbell DG, Deak M, Ordureau A, Macartney T, Tong Y, Shen J, Prescott AR, Alessi DR (2010) 14-3-3 binding to LRRK2 is disrupted by multiple Parkinson's disease-associated mutations and regulates cytoplasmic localization. Biochem J 430:393–404. CrossRef Medline

Ostrerova N, Petrucelli L, Farrer M, Mehta N, Choi P, Hardy J, Wolozin B (1999) α-Synuclein shares physical and functional homology with 14-3-3 proteins. J Neurosci 19:5782–5791. CrossRef Medline

Park JW, Vahidi B, Taylor AM, Rhee SW, Jeon NL (2006) Microfluidic culture platform for neuroscience research. Nat Protoc 1:2128–2136. CrossRef Medline

Paumier KL, Luk KC, Manfredsson FP, Kanaan NM, Lipton JW, Collier TJ, Steece-Collier K, Kemp CJ, Celano S, Schulz E, Sandoval IM, Fleming S, Dirr E, Polinski NK, Trojanowski JQ, Lee VM, Sortwell CE (2015) Intrastriatal injection of pre-formed mouse alpha-synuclein fibrils into rats triggers alpha-synuclein pathology and bilateral nigrostriatal degeneration. Neurobiol Dis 82:185–199. CrossRef Medline

Plotegher N, Kumar D, Tessari I, Brucale M, Munari F, Tosatto L, Belluzzi E, Greggio E, Bisaglia M, Capaldi S, Aioanei D, Mammi S, Monaco HL, Samo B, Bubacco L (2014) The chaperone-like protein 14-3-3η interacts with human alpha-synuclein aggregation intermediates rerouting the amyloidogenic pathway and reducing alpha-synuclein cellular toxicity. Hum Mol Genet 23:5615–5629. CrossRef Medline

Porter GW, Khuri FR, Fu H (2006) Dynamic 14-3-3/client protein interactions integrate survival and apoptotic pathways. Semin Cancer Biol 16: 193–202. CrossRef Medline

Qiao H, Foote M, Graham K, Wu Y, Zhou Y (2014) 14-3-3 proteins are required for hippocampal long-term potentiation and associative learning and memory. J Neurosci 34:4801–4808. CrossRef Medline

Ramser EM, Buck F, Schachner M, Tilling T (2010) Binding of alphaII spectrin to 14-3-3β is involved in NCAM-dependent neurite outgrowth. Mol Cell Neurosci 45:66–74. CrossRef Medline

Sato S, Chiba T, Sakata E, Kato K, Mizuno Y, Hattori N, Tanaka K (2006) 14-3-3η is a novel regulator of parkin ubiquitin ligase. EMBO J 25:211–221. CrossRef Medline

Schneider CA, Rasband WS, Eliceiri KW (2012) NIH image to ImageJ: 25 years of image analysis. Nat Methods 9:671–675. CrossRef Medline

Shahnawaz M, Tokuda T, Waragai M, Mendez N, Ishii R, Trenkwalder C, Mollenhauer B, Soto C (2017) Development of a biochemical diagnosis of parkinson disease by detection of α-synuclein misfolded aggregates in cerebrospinal fluid. JAMA Neurol 74:163–172. CrossRef Medline

Shandala T, Woodcock JM, Ng Y, Biggs L, Skoulakis EM, Brooks DA, Lopez AF (2011) *Drosophila* 14-3-3ε has a crucial role in anti-microbial peptide secretion and innate immunity. J Cell Sci 124:2165–2174. CrossRef Medline

Shin KJ, Wall EA, Zavzavadjian JR, Santat LA, Liu J, Hwang JI, Rebres R, Roach T, Seaman W, Simon MI, Fraser ID (2006) A single lentiviral vector platform for microRNA-based conditional RNA interference and coordinated transgene expression. Proc Natl Acad Sci U S A 103:13759–13764. CrossRef Medline

Slone SR, Lesort M, Yacoubian TA (2011) 14-3-3θ protects against neurotoxicity in a cellular Parkinson's disease model through inhibition of the apoptotic factor bax. PLoS One 6:e21720. CrossRef Medline

Slone SR, Lavalley N, McFerrin M, Wang B, Yacoubian TA (2015) Increased 14-3-3 phosphorylation observed in Parkinson's disease reduces neuroprotective potential of 14-3-3 proteins. Neurobiol Dis 79:1–13. CrossRef Medline

Sluchanko NN, Gusev NB (2017) Moonlighting chaperone-like activity of the universal regulatory 14-3-3 proteins. FEBS J 284:1279–1295. CrossRef Medline

Stuendl A, Kunadt M, Kruse N, Bartels C, Moebius W, Danzer KM, Mollenhauer B, Schneider A (2016) Induction of α-synuclein aggregate formation by CSF exosomes from patients with Parkinson's disease and dementia with Lewy bodies. Brain 139:481–494. CrossRef Medline

Tan CC, Yu JT, Tan MS, Jiang T, Zhu XC, Tan L (2014) Autophagy in aging and neurodegenerative diseases: implications for pathogenesis and therapy. Neurobiology of aging 35:941–957. CrossRef Medline

Théry C, Amigorena S, Raposo G, Clayton A (2006) Isolation and characterization of exosomes from cell culture supernatants and biological fluids. Curr Protoc Cell Biol Chapter 3: Unit 3 22. CrossRef Medline

Tonoki A, Kuranaga E, Tomioka T, Hamazaki J, Murata S, Tanaka K, Miura M (2009) Genetic evidence linking age-dependent attenuation of the 26S proteasome with the aging process. Mol Cell Biol 29:1095–1106. CrossRef Medline

Ulitsky I, Krishnamurthy A, Karp RM, Shamir R (2010) DEGAS: de novo discovery of dysregulated pathways in human diseases. PLoS One 5:e13367. CrossRef Medline

VanGuilder HD, Farley JA, Yan H, Van Kirk CA, Mitschelen M, Sonntag WE, Freeman WM (2011) Hippocampal dysregulation of synaptic plasticity-associated proteins with age-related cognitive decline. Neurobiol Dis 43:201–212. CrossRef Medline

Vincenz C, Dixit VM (1996) 14-3-3 proteins associate with A20 in an isoform-specific manner and function both as chaperone and adapter molecules. J Biol Chem 271:20029–20034. CrossRef Medline

Volpicelli-Daley LA, Luk KC, Patel TP, Tanik SA, Riddle DM, Stieber A, Meaney DF, Trojanowski JQ, Lee VM (2011) Exogenous alpha-synuclein fibrils induce Lewy body pathology leading to synaptic dysfunction and neuron death. Neuron 72:57–71. CrossRef Medline

Volpicelli-Daley LA, Luk KC, Lee VM (2014) Addition of exogenous α-synuclein preformed fibrils to primary neuronal cultures to seed recruitment of endogenous α-synuclein to Lewy body and Lewy neurite-like aggregates. Nat Protoc 9:2135–2146. CrossRef Medline

Winter JF, Höpfner S, Korn K, Farnung BO, Bradshaw CR, Marsico G, Volkmer M, Habermann B, Zerial M (2012) Caenorhabditis elegans screen reveals role of PAR-5 in RAB-11-recycling endosome positioning and apicobasal cell polarity. Nat Cell Biol 14:666–676. CrossRef Medline

Xu J, Kao SY, Lee FJ, Song W, Jin LW, Yankner BA (2002) Dopamine-dependent neurotoxicity of α-synuclein: a mechanism for selective neurodegeneration in Parkinson disease. Nat Med 8:600–606. CrossRef Medline

Yacoubian TA, Cantuti-Castelvetri I, Bouzou B, Asteris G, McLean PJ, Hyman BT, Standaert DG (2008) Transcriptional dysregulation in a transgenic model of parkinson disease. Neurobiol Dis 29:515–528. CrossRef Medline

Yacoubian TA, Slone SR, Harrington AJ, Hamamichi S, Schieltz JM, Caldwell KA, Caldwell GA, Standaert DG (2010) Differential neuroprotective effects of 14-3-3 proteins in models of Parkinson's disease. Cell Death Dis 1:e2. CrossRef Medline

Yamaguchi O, Otsu K (2012) Role of autophagy in aging. J Cardiovasc Pharmacol 60:242–247. CrossRef Medline

Yano M, Nakamuta S, Wu X, Okumura Y, Kido H (2006) A novel function of 14-3-3 protein: 14-3-3ζ is a heat-shock-related molecular chaperone that dissolves thermal-aggregated proteins. Mol Biol Cell 17:4769–4779. CrossRef Medline

Yoon BC, Zivraj KH, Strochlic L, Holt CE (2012) 14-3-3 proteins regulate retinal axon growth by modulating ADF/cofilin activity. Dev Neurobiol 72:600–614. CrossRef Medline